Geochemical controls and characteristics of natural seepage of carbon dioxide along the Bongwana Fault, KwaZulu-Natal and Eastern Cape Provinces

UNIVERSITY OF THE
WITWATERSRAND,
JOHANNESBURG

HYDROGEOLOGY RESEARCH REPORT (GEOL7028)

Submitted by

Jabulani Justice Sello

555591

Supervisor: Professor Tamiru Abiye

A Research Report submitted to the Faculty of Science, University of the Witwatersrand, in partial fulfilment of the requirements for the degree of Master of Science in Hydrogeology, School of Geosciences

October 2019

Declaration

I, **Jabulani Justice Sello**, declare that this report is my own, original unaided work. It is being submitted in partial fulfilment of the requirements for the degree of Master of Science in Hydrogeology at the Faculty of Science, University of the Witwatersrand, Johannesburg. It has not been submitted before for any degree or examination in any other University.

Jabulani Justice Sello

Signed at Johannesburg on the 29th of October 2019

Abstract

This study was intended to investigate the major geochemical processes controlling the aqueous CO_2 detected in selected sampling points along the Bongwana Fault, considering the characteristics and potential impacts thereof. Various complementary methods were used to identify the major geochemical processes governing the chemical compositions of the waters in the study area. These include isotope analysis, classification of water facies, stoichiometric and bivariate analysis for water-rock interactions assessment and geochemical modelling (determination of mineral Saturation Indices).

The $\delta^{18}O$ and $\delta^{2}H$ isotopes indicated that there is mixing of connate and recently recharged waters in the groundwater system. However, poor construction of Bongwana boreholes overemphasises the rate of recharge in the sampling area as the boreholes allow rainwater to percolate and dilute the preserved compositions during periods of heavy rainfall.

The source of CO_2 in the area was investigated using $\delta^{13}C$ and results revealed the source to be carbonate dissolution attributed to the reaction of acidic groundwater with the Marble Delta Formation carbonate rocks. Further analysis indicated that carbonate dissolution is coupled and interchangeable with calcite re-precipitation to form the travertines that were seen covering the surfaces in Umtamvuna and Bongwana areas as a result of CO_2 degassing. Carbonate dissolution under the influence of temperature, pH, saturation states and pCO_2 is the principal geochemical process controlling the observed chemical compositions as free Ca^{2+} and HCO_3^- are released in solution. Geochemical modelling indicated that calcite is oversaturated with respect to the solution it is contained in; hence more travertine will continue to form from saturated groundwater in Umtamvuna. Moreover, geochemical modelling also shows CO_2 will be released without forming any travertine surfaces in Bongwana since calcite is undersaturated and is less likely to precipitate.

The Msikaba Formation sandstone is the main aquifer in the study area and is influenced by connate waters of marine origin, introducing high concentrations of Na^+, Cl^- and SO_4^{2-}. Water-rock interaction indicated that reverse ion exchange is prevalent which resulted in the exchange of Ca and Na as indicated by the following dominant water facies: Na-Mg-HCO_3-Cl and Na-Mg-HCO_3-Cl-SO_4 driven by halite dissolution. Umtamvuna groundwater are ionically related and connected at depth through fractures.

Keywords: Bongwana, CO_2, geochemical processes, geochemical modelling, carbonate dissolution, isotopes, water facies, water-rock interactions.

Acknowledgements

I would like to express my most sincere gratitude to my academic supervisor, Professor Tamiru Abiye for guidance and being patient with me throughout the course of this programme. I would also like to extend my gratitude to (1) Mr. Blessing Mbonani of the University of Pretoria for being my driver to and from fieldwork, (2) Miss Despina Tshipala for sharing knowledge whenever I bothered her with questions, (3) Dr. Stephanie Scheiber-Enslin for her assistance with working around the software I needed to process my results and (4) Miss Mandy-Jane Sebola for assisting me with quality edit of draft. I would like to acknowledge and thank Mr. Mike Butler from iThemba Labs for his dedication to assisting with isotope analysis which was instrumental for this research.

Special thanks principally to the following parties: South African National Energy Development Institute (SANEDI) – in particular to Mr. Thabo Mosia for making it easier for me to get assistance with everything I needed and the 10-star treatment. National Research Foundation (NRF) and the Council for Geoscience (CGS) with the provision of additional support and data. Not forgetting the handy assistance of the community of Bizana men who graciously walked up and down the Umtamvuna near-vertical steep heels carrying containers full of sampled water needed for the analysis as part of stakeholder engagement through SANEDI.

Family support doesn't go unnoticed. After all, they are the reason why I did this.

Last but not least, I would like to thank myself for soldering on through this whole research, for staying disciplined even when there was not motivation to carry on work.

Table of Contents

List of Abbreviations and Acronyms

CAI	Chloro-alkaline indices
CCS	Carbon capture and storage
CGS	Council for Geosciences
DIC	Dissolved Inorganic Carbon
DO	Dissolved Oxygen
EC	Electrical Conductivity
ECP	Eastern Cape Province
GMWL	Global Meteoric Water Line
IAEA	International Atomic Energy Agency
KZN	KwaZulu-Natal
LMWL	Local meteoric water line
PDB	Pee Bee Belemnite
PHREEQC	pH Reaction Equilibrium Calculation
pMC	Percentage modern carbon
PTFE	Polytetrafluoroethylene
SACCCS	South African Centre for Carbon Capture and Storage
SANEDI	South African National Energy Development Institute
SI	Saturation Indices
SMOW	Standard Mean Ocean Water
TDS	Total Dissolved Solids

List of Figures

List of Tables

Chapter 1: Introduction

Human-induced carbon dioxide plays the most significant role in climate change as one of the greenhouse gases emitted into the atmosphere (Metz *et al*. 2005; Fischer, 2011). However, electricity generation by coal combustion remains the leading contributor to greenhouse gas emissions in South Africa (Metz *et al*. 2005). Despite the Government's commitment to reduce emissions by developing clean and renewable energy technologies, coal remains in high demand (Metz *et al*. 2005; Fischer, 2011). In 2017, it was reported that South Africa's coal export and usage was expected to expand from 4 million to 38 million tonnes per year by year 2030 (Kretzmann, 2017). The South African government has and continues to develop clean and renewable energy technologies. Nonetheless, it has been demonstrated that we still rely heavily on fossil fuels such as coal for electricity generation which has contributed vastly to a slow release in gas emissions to the atmosphere (Urban Earth, 2012). In recent years, carbon capture and storage (CCS) has emerged as an effective method of alleviating the adverse effects associated with burning fossil fuels (Beck *et al*. 2013). Several countries such as Norway have successfully adopted this method to allow for sustainable and cleaner usage of coal as the primary fossil fuel while mitigating against global climate change (Gavenas *et al*. 2015). Given this success and the fact that South Africa is endowed with relatively stable geological conditions, CCS is likely to be a viable method of reducing greenhouse gas emissions (Beck *et al*. 2013).

According to Hicks *et al*. (2014) South Africa is in dire need of a portfolio of technological solutions that will be used to reduce carbon dioxide pollution, with CCS becoming the most crucial technology of this portfolio. There is insufficient background knowledge on the potential of CCS technology in South Africa due to limited historical data (Hicks *et al*. 2014; Bond *et al*. 2017).

The current focus on CCS research is concentrated on carbon dioxide sequestration in the Earth's sub-surface formations such as depleted oil and gas sedimentary basins, with the Zululand Basin being a primary example (Bond *et al*. 2016; Bond *et al*. 2017). Nonetheless, potential issues related to storing carbon dioxide in the geological formations include long-term assessment (of a suitable place for storing carbon dioxide) and monitoring with unknown adverse impacts that are yet to be determined (Bond *et al*. 2016; Bond *et al*. 2017).

In order to facilitate the successful implementation of CCS technologies in South Africa, it is crucial to have a deeper understanding of the science and impacts associated with this technology. This can be achieved by studying the pre-existing natural CO_2 seepage sites as they mimic the physical conditions at which CO_2 is stored within rock formations (Bond *et al*. 2017).

The South African Centre for Carbon Capture and Storage (SACCCS) whose mother body is the South African National Energy Development Institute (SANEDI), under the authority of the Department of Energy has been appointed in partnership with the Council for Geosciences (CGS) to spearhead the implementation and development of CCS in South Africa as of 2010. These stakeholders have launched a pilot CO_2 project in the Zululand Basin situated near the Mozambique Basin as of 2018 and will continue into 2022 (Beck *et al*. 2013; Hicks *et al*. 2014). A complementary project has already commenced, monitoring natural CO_2 seepage in Bongwana – approximately 530 kilometres south-west of the Zululand Basin (Hicks *et al*. 2014; Hicks, 2015).

In conjunction with the ongoing research, the present study investigated sites within Bongwana where natural carbon dioxide is released with the purpose of characterising the gas, its geochemical controls and interaction with the surrounding environment.

1.1. Background

The process of securely sequestrating CO_2 into geological reservoirs requires new CCS technologies to be developed such that they incorporate monitoring systems that allow the identification of probable leakages from the target reservoir (Johnson *et al*. 2017). However, it must be noted that since each geological setting is unique, it is crucial to fully assess the compatibility of the monitoring technologies such as soil gas fluxes on the basis of their precise and accurate detection of any likely CO_2 leakages and, also to fully comprehend probable leakage pathways and their structures with the purpose of successful implementation of appropriate monitoring plans (Ringrose *et al*. 2013; Johnson *et al*. 2017). Two situations that characterise CO_2 storage failure and leakage are (1) sudden leakage attributed to injection well failure or a deserted well, and (2), progressive leakage through undiscovered faults and fractures (Metz *et al*. 2005; Johnson *et al*. 2017).

The second CO_2 storage failure scenario was of particular interest for the present study because the new knowledge generated will improve the understanding, development and verification of CCS research South Africa. Hence, the study focused on gradual CO_2 leakage through a preferential network of fluid-flow pathways such as fractures or faults. This approach enabled the understanding of the role, impact and implications of these flow pathways on CCS integrity (Bond *et al*., 2016; Bond *et al*. 2017).

Gradual leakage of CO_2 (to the surface environment) controlled by fractures, faults and other flow pathways has been identified as the leading source of negative perceptions that the general public and different organisations have towards the CCS technology (Bond *et al*. 2017). For example, an ongoing CO_2 injection was interrupted at a CCS pilot site situated at Ain Salah, Algeria as a result of fractures

which were developed and progressed as a conductive network transporting CO_2 back to the surface (see Bond *et al*. 2013; Rinaldi and Rutqvist, 2013; Ringrose *et al*. 2013).

To overcome this problem in South Africa, SANEDI on behalf of the South African government and all involved governing and funding organisations, has established a stakeholder engagement plan where all the people who may be affected by the CCS project are given the opportunity to voice their concerns. This was done through transparent exchange and disclosure of any information related to the planned CCS pilot project in their respective areas and thereafter decisions could be made in terms of finding a way forward. Communication with the affected parties is conducted based on social hierarchy whereby representatives from the district and local municipalities, traditional leaders and lastly, the local residents.

1.2. Present Study's Implication for CCS Development and the Significance of Monitoring in South Africa

Given the fact that most parts of South Africa are water-stressed, it became imperative to give the proposed CCS pilot and monitoring projects necessary attention as their success is dependent on the usage of primary aquifers that happen to be the source of freshwater needed to sustain life. The principal disadvantage of injecting CO_2 into a sub-surface geological reservoir is the possibility of leakage and impact onto the freshwater and the environment. Elevated dissolved CO_2 introduces acidity into the freshwater resources through the formation of carbonic acid as the water pH is lowered. Most heavy metals become mobile at low pH levels hence, can run the risk of acid mine drainage if an aquifer undergoes mineral leaching. A pH shift can also be undesirable for the pH-sensitive ecosystem.

Therefore, it is crucial to monitor this natural CO_2 release and learn how CO_2 interacts with the environment with the purpose of being able to plan how to protect the environment against any potential unintended CCS failures.

1.3. Study Area

The study area (Figure 1) is located in the Bongwana gas fault, which is an approximately north-south trending fault that can be traced for about 80 kilometres (De Decker, 1981; Harris *et al*. 1997). This fault has a N-S trend in parts of Kwa-Zulu Natal Province extending into the Eastern Cape Province. The Bongwana Fault is the longest in the region, taking into consideration its relation to the flexural monocline along the Kwa-Zulu Natal coast (Harris *et al*. 1997). De Decker (1981) approximated that the vertical motion along the fault is about 550 metres in the centre.

The Bongwana Fault is distinctly marked by points where natural CO_2 is released to the surface through fractures, mound, and travertine cone-springs (Figure 1) (Bond *et al*. 2017). The release of CO_2 from these passageways was first documented in the 20th century (du Toit, 1920; Young, 1924; Gevers, 1941; du Toit, 1946), resulting in the establishment of a gas-bottling company to exploit dry CO_2 (Harris *et al*. 1997; Bond *et al*. 2017; Johnson *et al*. 2017).

Although the Bongwana Fault runs along several areas, it is mostly well-studied in the Bizana village, which falls under the Alfred Nzo District Municipality in the Eastern Cape Province, as well as Bongwana village falling under Ugu District Municipality in KwaZulu-Natal. The CO_2 exhalations are well documented in these areas (Hicks *et al*. 2015). Most of the natural CO_2 exhalation sites (from Bongwana to Bizana) were only identified along the N-S trend after the CO_2 commercial gas-bottling plant was first established in Bongwana. The exhalation sites coincide with and appear to be structurally controlled by Bongwan-Ntlakwe Fault (du Toit, 1920; Gevers, 1941; Bond *et al*. 2016; Johnson *et al*. 2017).

SANEDI, with the assistance of previous studies in the region, has been able to compile information pertaining to the exact location of field sites where CO_2 exhalations can be studied. These areas are (i) Umtamvuna in Bizana, Eastern Cape, (ii) Baker's Farm and (iii) Manzimhlanga wherein the latter two are situated in Kwa-Zulu Natal. For this study, measurements and observations were only done in Bizana and Baker's Farm due to restricted access to the now privately-owned farms.

Fracturing and faulting in Bizana and Baker's Farm have led to the seepage of a spring line along the fault/fracture surface and acts as a barrier to the flow of water and CO_2 in the case where the precipitation of calcite cement the fractures or the fault (Bond *et al*. 2017). Most of the areas where historical work was done (Figure 1-d), were not re-visited for the present study because the CO_2 gas releases are no longer present.

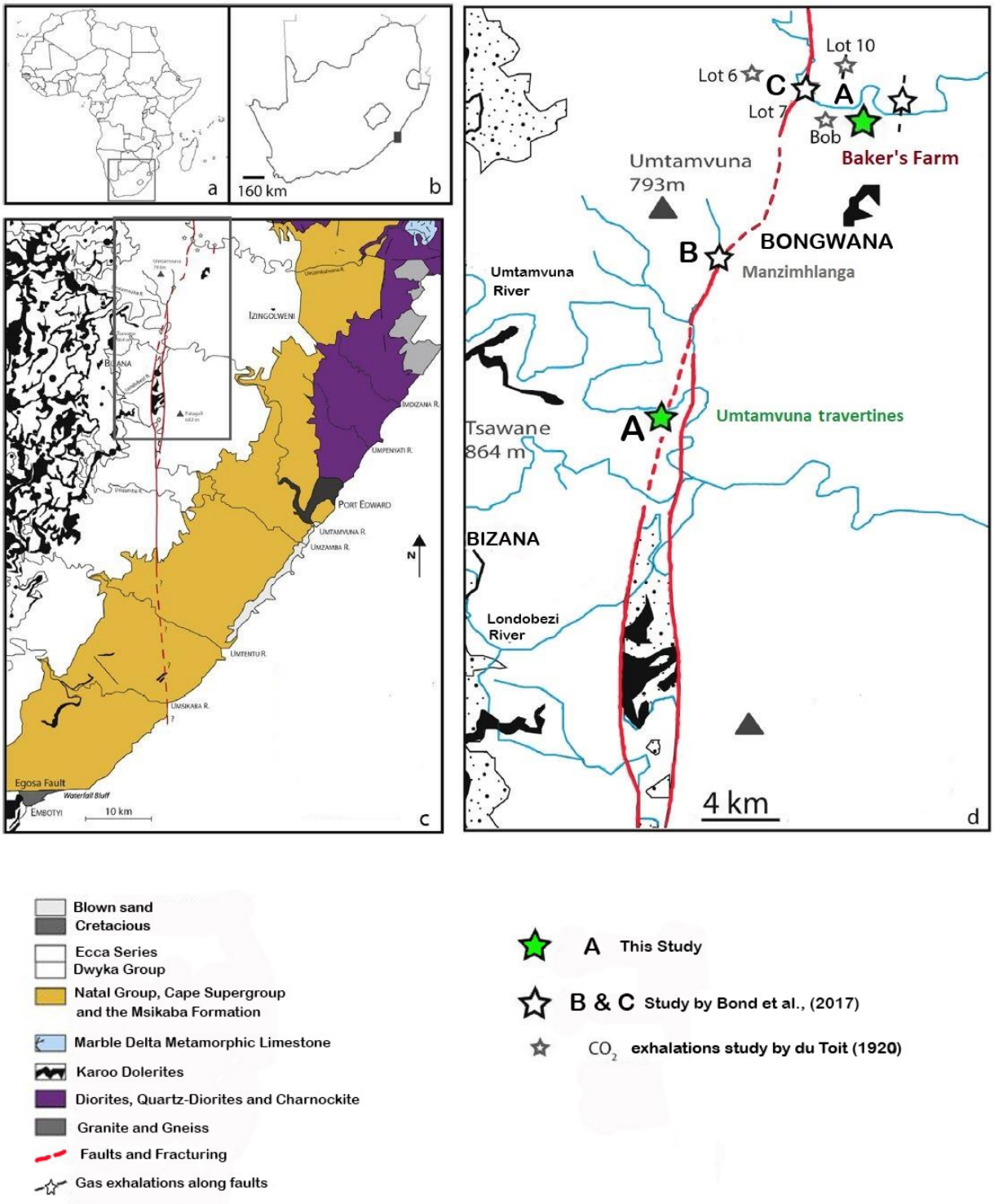

Figure 1: Location map and the generalized geology of the study area (Source: Bond *et al*. 2017).

1.3.1. Umtamvuna in Bizana

This area, situated approximately 14 km SSW of Bongwana, is characterised by the presence of travertine cones and mound springs varying in diameter from 1 to 15 metres (Figures 2.1, 2.2 and 2.3), which were developed along the banks of the Umtamvuna river separating the Eastern Cape Province from KwaZulu-Natal Province (Gevers, 1941; Hicks *et al*. 2015; Johnson *et al*. 2017). Johnson *et al*. (2017) further indicated that the Umtamvuna cones are popular sites of CO_2 exhalations along the southernmost part of the fault system. The spring site is underlain by Dwyka Group tillites of the Karoo Supergroup on the northern edge of an extensive graben system where the mapped Bongwan-Ntlakwe fault veers into two splays marked by a central collapse (Johnson *et al*. 2006; Johnson *et al*. 2017).

The springs originate from fractures linked to the main Bongwana Fault, where dissolved CO_2 is found to be bubbling from the springs. Some of the CO_2 were detected in the Umtamvuna stream water (Hicks *et al*. 2014; Hicks, 2015; Johnson *et al*. 2017). The northern part of the river bank is characterised by the presence of the largest cones in the area (about 15 metres in diameter) and are less active, whereas the smallest cones (1 meter in diameter and about 80 cm in height) occur on the southern part of the river bank and they were found to be releasing the high CO_2 when compared to those on the northern bank, see Figures 2.1, 2.2 and 2.3. (Gevers, 1941; Johnson *et al*. 2017). By observations, some of the smaller springs which occurred in clusters around the main springs have since been dormant (or probably became extinct) as a result of sealing attributed to visible calcite cementation along smaller fractures over time (Bond *et al*. 2017).

1.3.2. Baker's Farm

Bakers Farm is situated in the Bongwana village, south of Harding, Kwa-Zulu Natal and it lies approximately 4 km east-south-east of the historic commercial CO_2 bottling plant and CO_2 exhalations that were first mapped and documented by du Toit (1920). Bakers Farm is a relatively newly discovered area as far as research on the natural release of CO_2 in South Africa is concerned. The site was discovered before 2014 after CO_2 was intersected at a depth of 60 m when local farm owners drilled a borehole for domestic purposes. The borehole had since been collared, cased and abandoned by the owners shortly after drilling (Johnson *et al*. 2017). Comparatively, no CO_2 was encountered at another borehole located 180 metres westwards from the CO_2-rich borehole. Water samples from both boreholes were sampled to allow for comparison in this study.

1.3.3. Manzimhlanga

Another location of historic CO_2 releases is Manzimhlanga, situated approximately 8 km south west of Bongwana (denoted star symbol B in Figure 1). Although Gevers (1941) documented very small occurrences of CO_2 along the banks of Manzimhlanga River during visits conducted in 1939 and 1940 respectively, Johnson *et al*. (2017) claimed that no actual work was done in this area since Young (1924) visited the area. For the present study no sampling was done in the area due to restricted access to the area by the property owners.

Figure 2.1: Travertine cone spring (southern bank) in Umtamvuna, Bizana.

Figure 2.2: A detailed view of the southern bank travertine cone spring. It is one of the most active as noted by the CO_2 bubbles in the spring water.

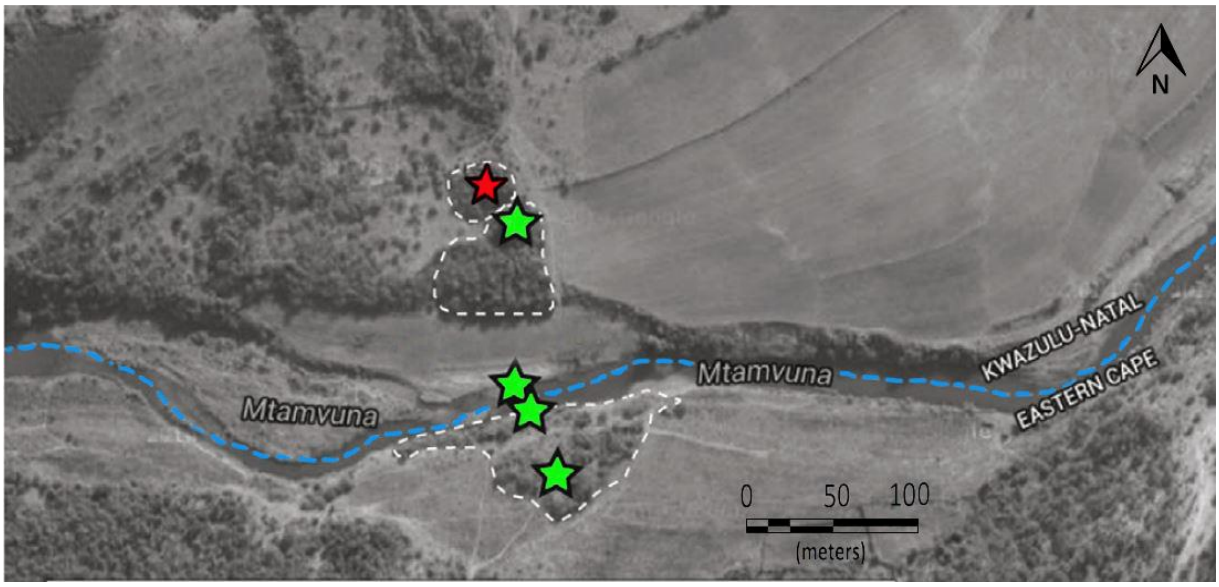

Figure 2.3: An aerial view of locations where CO_2 is released naturally in Umtamvuna. Green stars symbolize active travertine springs and the red star symbolizes dormant/extinct travertine springs. The areas demarcated by the white dashed lines denote the outline of the travertine outcrop. Image modified after Bond *et al*. (2017).

1.4. Aim of the Study

This research was aimed at understanding and modelling the hydrochemical changes associated with the groundwater in Bongwana, KwaZulu-Natal and Eastern Cape Provinces. The objectives addressed by the study include quantification of information on the source of CO_2 detected in the groundwater of the study area, assessment of the groundwater chemistry and an attempt to determine the relative circulation time of the groundwater. It is anticipated that the data generated from this research will contribute to the understanding of the chemical controls on the groundwater (and CO_2 by association) in the study area, so as to contribute knowledge towards the development of monitoring technology methods for CCS in South Africa.

Chapter 2: Climate, Land-use and Topography

2.1. Climate

The climatic conditions along the Bongwana Fault region are generally warm, temperate and fall within the summer rainfall regions (Climate Data, 2018). The region is characterised by significant precipitation (average 865 mm per year). Precipitation is highest in summer and lowest in winter (Figure 3-a). The data shows that precipitation is lowest in July (~17 mm) and highest in December-January (~130 mm). The temperatures in the region averages at 17.0℃ monthly, and are the highest in summer during the rainy season and lowest in winter during the dry season with limited rainfall (Figure 3-b). The region is generally humid and is dominated by subtropical weathering (Grab and Knight, 2015).

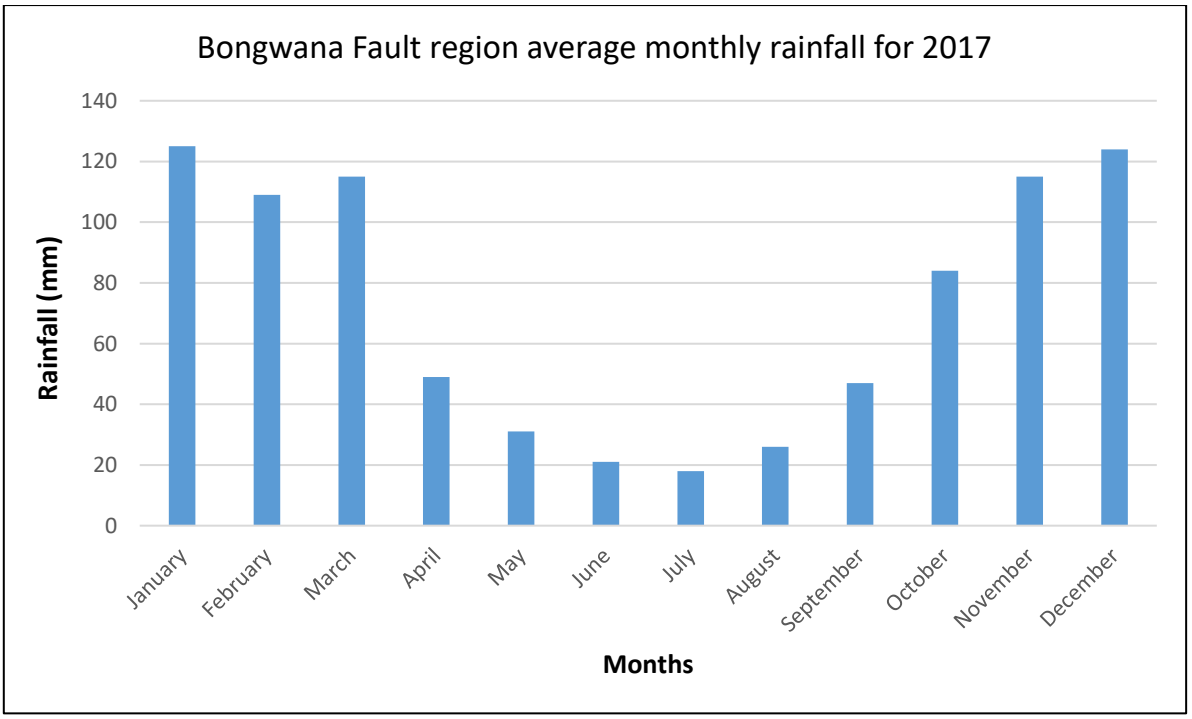

Figure 3-a: Average monthly rainfall for the study area for the 2017 year.

During the hottest month (January), average surface temperatures can reach up to about 35 ℃ mid-day (noon) until about 3 pm, whereas temperatures can drop to ~4 ℃ during the coldest winter month (July) (Climate Data, 2018).

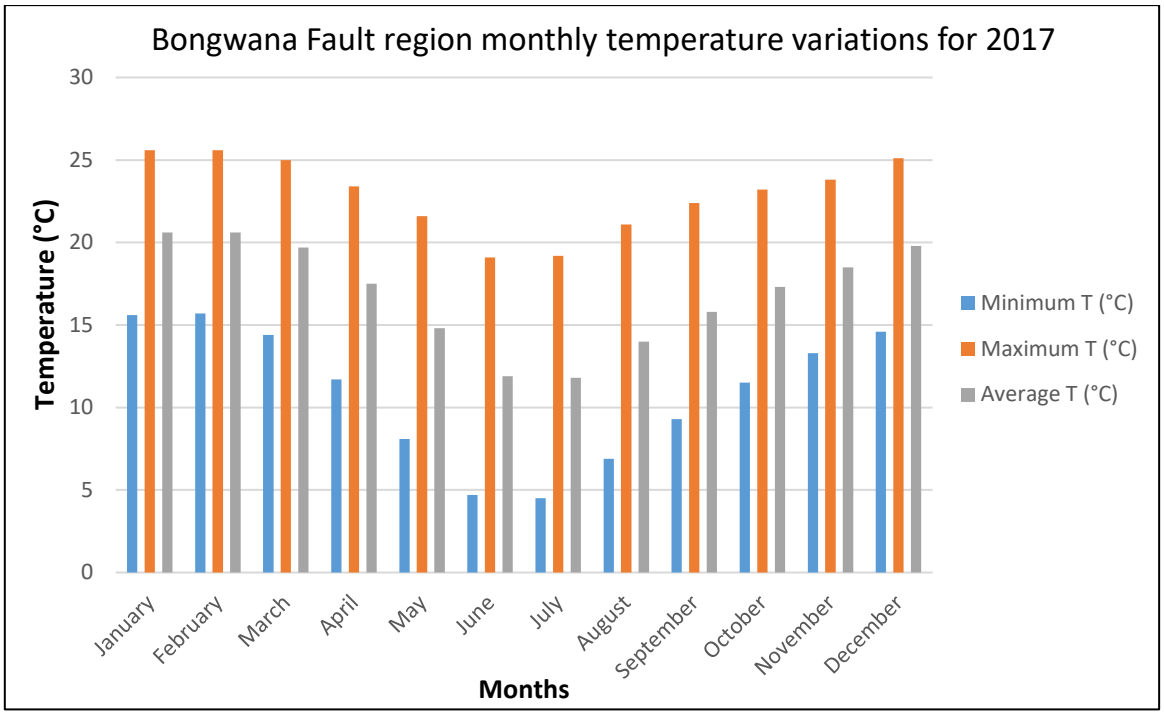

Figure 3-b: Average monthly temperature variations within the study area for 2017.

2.2. Topography and Land-cover/Land-use

The study area is dominated by twelve different types of vegetation, which include wide varieties of medicinal plants (Thornhill and van Vuuren, 2015). Thornhill and van Vuuren (2015) further reported that in general, the region is dominated by mangroves and a vast number of shrubs which are sensitive to the local climate since the region is situated in the sub-tropic zone. The general topography is relatively flat owing to the proximity near to the sea and becomes steeper when moving further inland. However, in Umtamvuna the springs are located along the banks of the Umtamvuna River, which flows within one of the biggest gorges in the region – the other being the famous Oribi Gorge situated about 20 km east of the study area, known for its nature reserve, zip-line and thus, a big tourist attraction in the region. The presence of these near-vertical hill slopes made sampling in Umtamvuna difficult, whereas sampling in Bongwana was easier because the two boreholes sampled are drilled on a relatively flat surface (Figure 4).

The region is dominated by the agricultural activities owing to consistent climate that allows a lot of subtropical fruits to grow in the region, such as banana farms. In Umtamvuna, subsistence farming is the most predominant land-use whereby most of the cultivated fields are situated down-valley next to the Umtamvuna River for easy access to the water needed for irrigation.

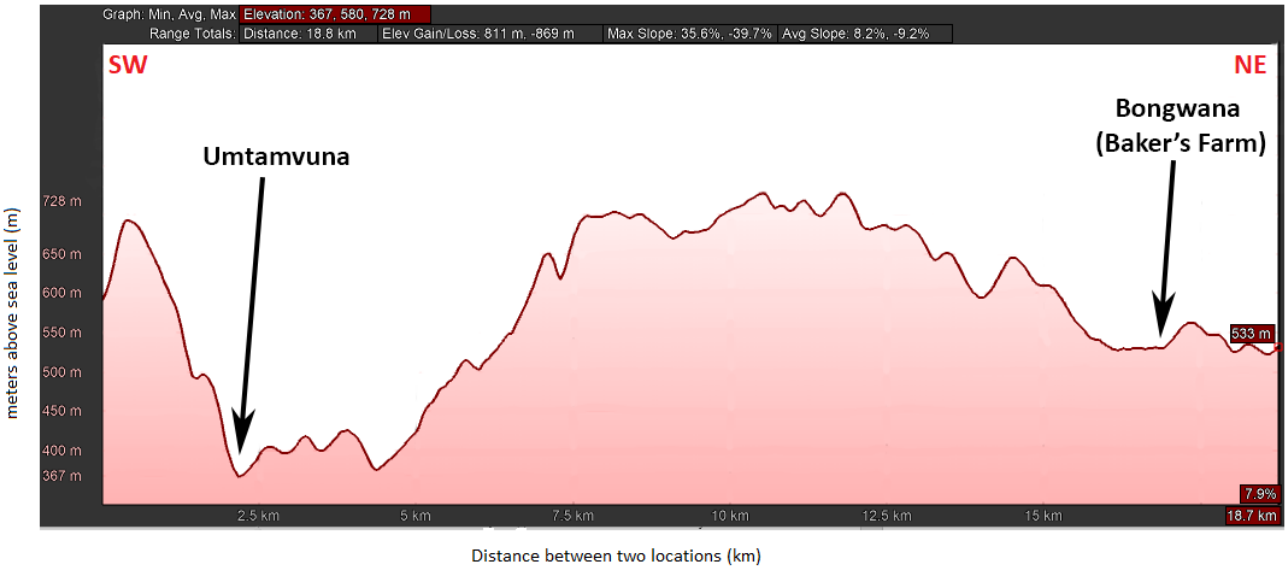

Figure 4: Cross-sectional view profile of the topography between the sampling points for this study.

Chapter 3: Geology of the Study Area

The Bongwana Fault also called Ntlakwe-Bongwan, was first discovered by du Toit (1920) while mapping Pondoland (now called Eastern Cape Province) and some sections of the lower uMzimkhulu and Alfred Counties (now called Port Shepstone). The fault cuts through the igneous and sedimentary rocks of the Karoo Supergroup, including rocks of the Msikaba Formation of the Cape Supergroup that outcrops from Hibberdene to Port Edward along the south-western coast of KwaZulu-Natal Province (Johnson *et al*., 2006; Busakwe, 2015; Bond *et al*. 2017). Minor shales and tillites of the Dwyka Group (Karoo Supergroup) make up the dominant rocks of the study area, see Figure 1 (Bond *et al*. 2017; Johnson *et al*. 2017). The Dwyka Group tillite with a thickness of approximately 450 metres in southern KZN, unconformably overlies the Natal Group and Msikaba Formation coarse-grained sandstones, conglomerates and minor shales, which subsequently overlies the gneiss and granite complex of the Mesoproterozoic Natal Metamorphic Province at depth, see Figure 5-a (Thomas *et al*. 1990; Johnson *et al*. 2006; Hicks, 2010; Johnson *et al*. 2017).

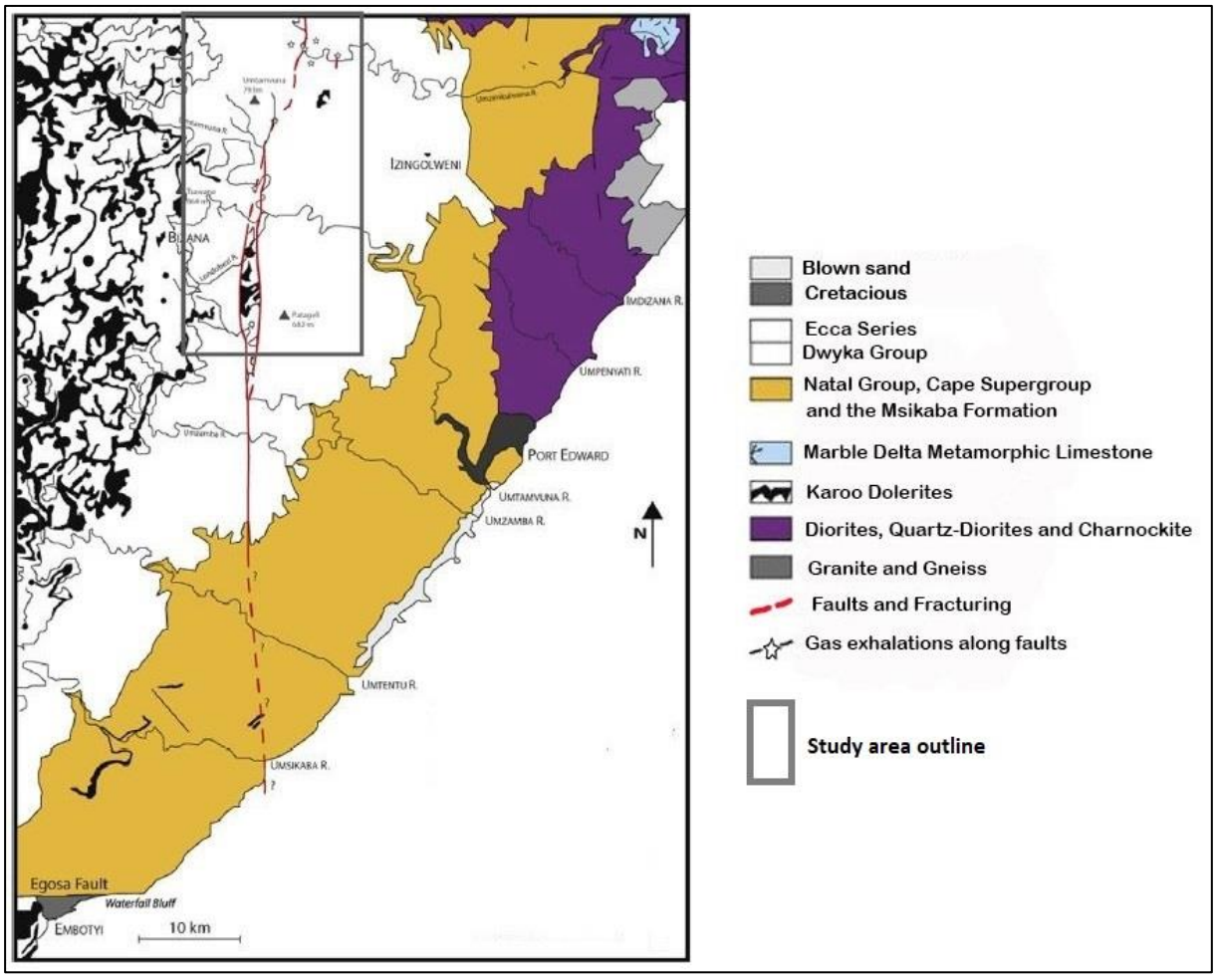

Figure 5-a: Geological map of the study area. Modified after Bond *et al*. (2017).

The Bongwana Fault cuts onto the surface along a trace that is approximately 80-kilometres long where its northern extension gave it the name Bongwana or Ntlakwe-Bongwan fault (De Decker, 1981; Harris *et al*. 1997; Hicks *et al.* 2015). Watkeys and Sokoutis (1998) stated that this fault is analogous to the Gondwana break-up which has been active for about 180 million years. The southern KwaZulu-Natal is marked by an approximately 70-kilometre-wide zone of deformation characterised by arching traces of faults that changed their ENE-WSW orientation and bent in an N-S fashion (Watkeys and Sokoutis, 1998; Watkeys, 2006; Bond *et al*. 2017). Bond *et al*. (2017) observed that faulting in this region concurs with the premature stage of arching, Type I fault system in the northern part of KwaZulu-Natal as defined by Von and Andersen (1990). See Figures 5-a and 5-b.

The fault trace within the study area is extremely difficult to find due to the uniform nature and extensive thickness of the observed tillite successions of the Dwyka Group. For this reason, there are no stratigraphic displacements that can be mapped within the sections of the study area that were visited (Figure 5-a). Bond *et al*. (2017) reported that southwards along the Londobezi river (Figure 1-d), a large graben structure that has formed between two splays of the Bongwana Fault. Moreover, the Karoo dolerite intrusion suites and sedimentary sequences (shales and sandstones) of the Ecca Group are still well-preserved along this graben (Bond *et al*. 2017). Work done by Duncan *et al*. (1997) suggest that faulting in the study area occurred at least approximately 179 million years ago, based on argon-argon ($^{40}\mathrm{Ar}/^{39}\mathrm{Ar}$) dating on the dolerite intrusion suite.

The Marble Delta Formation, seen outcropping about 30 km southeast of Bongwana Fault (Figures 1-c and 5-a) comprise predominantly of carbonate rocks as described in detail by Otto (1977) and Thomas and Otto (1991). Otto (1977) and Thomas and Otto (1991) stated that the Marble Delta Formation can be subdivided into the upper Oribi member made up of marine-sedimentary sequence calcite marble and the lower Le Jonquet member made up of dolomitic marble accompanied by a biogenic graphite, intercalated with quartzite and minor hematite. Furthermore, the calcite and dolomite marble is of a high grade and is thus, commercially exploited for cement production (Thomas and Otto, 1991). Common accessory minerals include phlogopite, forsterite and serpentine whereas minor amphibolite occur as a thin layer that overlies that calcite marble (Thomas and Otto, 1991).

In areas where the rocks are silica saturated and broken down into tiny angular fragments and cemented by fine-grained calcareous material, the fault trace is marked distinctly by a positive relief – this helps greatly with the interpretation of the faulting network (Thomas, 1988; Thomas *et al*., 1990; Bond *et al*. 2017). Gevers (1941); Bond *et al*. (2017) also reported that distinct zones of silicification mark the fault and fracture network in the study area, with an aperture ranging from 0.3 to 10 metres in width. Gevers (1941) further noted that the Dwyka tillite cropping up along the fault trace in the study area was

undergoing through intense chemical alteration as a result of alteration of feldspars and mica minerals to kaolinite under the influence of CO_2-rich groundwater seeping up to the surface (Figures 5-b and 5-c). Hence, kaolinization distinctly marks the fault zone in the study area as the tillite continues to get leached by CO_2-rich groundwater (Gevers, 1941).

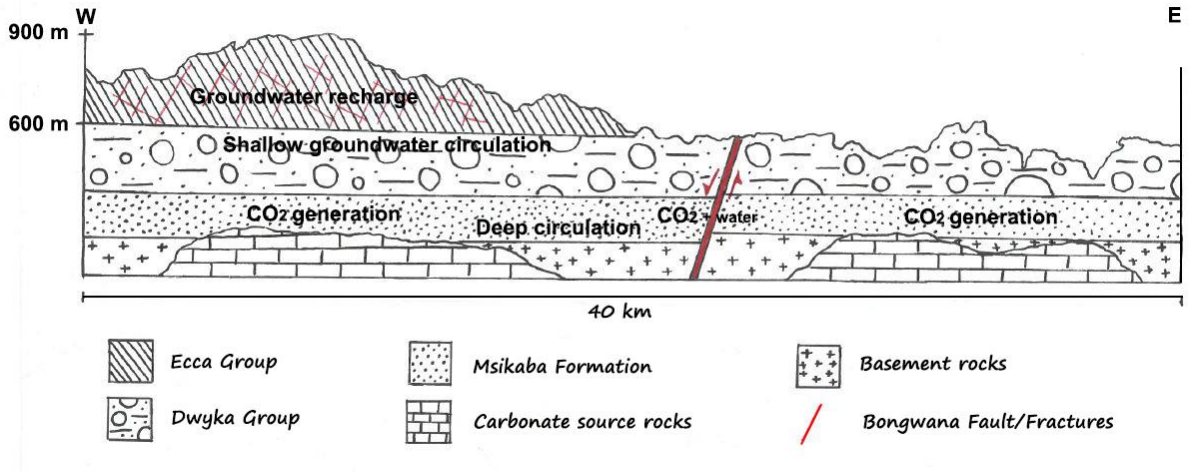

Figure 5-b: A geological cross-section of the study area (Source: Nkwane, 2018).

Figure 5-c: Pulverized Dwyka tillite that has undergone kaolinization (Source: Hicks *et al*., 2014).

Chapter 4: Methodologies

4.1. Materials and Methods

Several methods were engaged in this project, which include (1) field observations, (2) collection of water samples for major ion analysis, (3) collection of groundwater samples for isotope analysis, (4) measurements of physico-chemical parameters such as temperature, electrical conductivity (EC), pH, dissolved oxygen (DO), redox and Total Dissolved Solutes (TDS) and (5) the use of computer software to model hydrogeochemical variations in the groundwater.

4.1.1. Water Sampling Points

Nine water samples were collected; (4 samples from the travertine and mound springs in Umtamvuna, labelled TC-01, TC-02, TC-03 and UM-S respectively; 2 samples from CO_2-rich and CO_2-poor boreholes in Baker's Farm, labelled BH-01 and BH-02, respectively, and 3 river water samples labelled UM-F, UM-U and UM-D). All water samples were subjected to major ion analysis and isotope analysis.

TC-01 and TC-02 corresponds to the main travertine springs in the southern bank, TC-03 corresponds to the travertine cone situated on the other side of the river (northern bank), UM-S corresponding to the spring by the river bank, UM-F corresponding to the water samples taken from the river parallel to UM-S (this is the assumed fault trace running across the river in the area), UM-U corresponding to river water samples taken upstream and UM-D corresponding to river water samples taken downstream (Figure 5).

Table 1: Sampled water characteristics

Sample	Coordinates	Location	Borehole depth (m)	Surface elevation (m a. s. l.)	Depth to the water (m)	Water table elevation (m a. s. l.)
TC-01	30°48'31.57"S 29°57'45.43"E	Umtamvuna, Bizana, EC	-	367	N/A since water seeps up to the surface	-
TC-02	30°48'31.52"S 29°57'45.45"E	Umtamvuna, Bizana, EC	-	367	N/A since water seeps up to the surface	-
TC-03	30°48'28.02"S 29°57'45.66"E	Umtamvuna, Bizana, EC	-	362	N/A since water seeps up to the surface	-

UM-F	30°48'29.83"S 29°57'44.34"E	Umtamvuna, Bizana, EC	-	363	-	-
UM-S	30°48'30.14"S 29°57'44.74"E	Umtamvuna, Bizana, EC	-	366	N/A since water seeps up to the surface	-
UM-U	30°48'29.20"S 29°57'35.57"E	Umtamvuna, Bizana, EC	-	363	-	-
UM-D	30°48'29.44"S 29°57'49.95"E	Umtamvuna, Bizana, EC	-	363	-	-
BH-01	30°41'41.93"S 30° 2'29.31"E	Baker's Farm, Bongwana, KZN	60	560	48	512
BH-02	30°41'40.74"S 30° 2'24.40"E	Baker's Farm, Bongwana, KZN	60	544	54	490

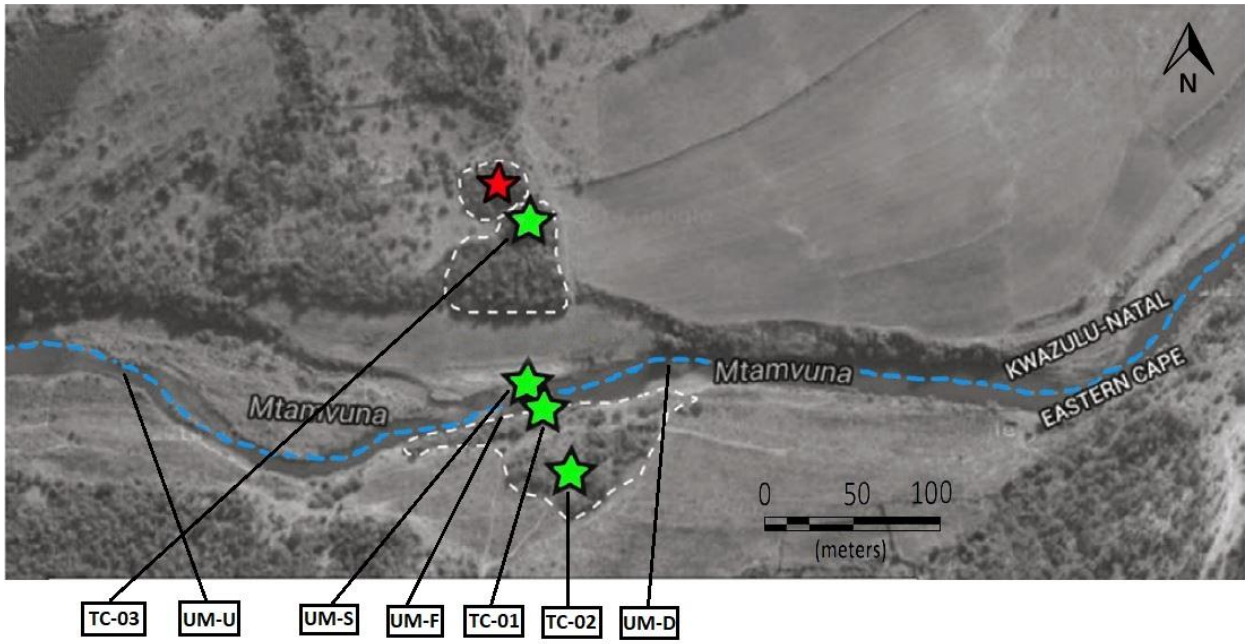

Figure 6: Location of sampling points in the Umtamvuna area.

4.1.2. Major Ion Analyses

For the determination of major ions, water sampling for cation analysis was done using a 100-ml bottle. The water samples were filtered using 0.45 µm filters. The samples were acidified with HNO_3 acid and were kept under cool temperatures. Water sampling for anion analysis was done using a 100 ml HDPE plastic bottles. Dionex QIC Ion Chromatograph (housed at CGS Pretoria head office) decked with an automated sampler, an IonPac AS4A analytical column and an IonPac AG4A guard column specifications, was used to measure the major ion analysis.

4.1.3. Isotope Analyses

The environmental isotopes analysed in this project include ^{18}O, ^{2}H, ^{13}C and ^{14}C.

The stable isotope analysis of ^{18}O and ^{2}H was carried out according to the method prescribed by Abiye *et al*. (2018). The method entailed using the Liquid Water Isotope Analyzer 45-EP housed at the Hydrogeology Lab, University of the Witwatersrand, Johannesburg. The instrument is equipped with a laser analysis system, an internal computer, a small membrane vacuum pump and an air room inlet that transmits air using a drierite column to remove moisture. Approximately 1 to 5 ml of a small sample (taken from a larger water sample) was transferred into a 2 ml vial using a pipette and sealed with polytetrafluoroethylene (PTFE) septum caps. A 0.75 µl of water sample was injected through a polytetrafluoroethylene in the auto-sampler using a Hamilton microliter ™ syringe. The auto-sampler injection port was heated to 46 ℃ with the purpose of vapourising the sample under vacuum immediately after injection. The vapour subsequently moves down through the transfer line into the void mirrored chamber where it was then analysed. The analytical procedure incorporated the use of 5 standards with known $\delta^{18}O$ and $\delta^{2}H$ values (5C: $\delta^{2}H$ − 9.2 ± 0.5‰, $\delta^{18}O$ − 2.69 ± 0.15‰, 4C: $\delta^{2}H$ − 51.6 ± 0.5‰, $\delta^{18}O$ − 7.94 ± 0.15‰, 3C: $\delta^{2}H$ − 97.3 ± 0.5‰, $\delta^{18}O$ − 13.39 ± 0.15‰, 2C: $\delta^{2}H$ −123.7 ± 0.5‰, $\delta^{18}O$ − 16.24 ± 0.15‰ and 1C: $\delta^{2}H$ − 154 ± 0.5‰, $\delta^{18}O$ − 19.49 ± 0.15‰). In addition, the laser analyser has an automatic calibration feature which allows it to give stable isotope values. The laser's maximum capacity allows it to give accurate results that are precise to roughly 1‰ for $\delta^{2}H$ and 0.2‰ for $\delta^{18}O$ in samples of water

The carbon-13 (^{13}C) of the samples taken can also be expressed also in a notation acceptable to the Vienna Pee Dee Belemnite (VPDB) introduced by Salem *et al*. (1980) as follows:

$$A_{init} \approx \frac{(\delta^{13}C_{DIC} - \delta^{13}C_{lime})}{\delta^{13}C_{CO_2} - \delta^{13}C_{lime} + \varepsilon_{CO_{2-lime}}} * 100 \text{ pMC} \quad (1)$$

Geyh (2000) stated that although Equation 1 is not theoretically appropriate, however it remains applicable since it takes into consideration the isotopic variations between CO_2 and $CaCO_3$, assuming that the system is closed. This is particularly relevant in this study since a carbonate-CO_2 system was being investigated.

Radiocarbon analysis was done at the iThemba Labs, Gauteng and was achieved through the drum precipitation field method where the objective was to acquire adequate carbon (minimum 2g) for the analysis. This procedure was ensured by addition of the following reagents: NaOH added to raise the pH of the sample water to make it alkaline and barium chloride ($BaCl_2$) to precipitate barium carbonate ($BaCO_3$) which was the final product taken for radiocarbon analysis. Phenolphthalein solution was added to attain check the desired pH. The solution was left overnight to allow the $BaCO_3$ to precipitate out of suspension and it was collected in a 1 litre plastic bottle for analysis. The analysis was also done at iThemba Labs, Gauteng, for carbon-13 and carbon-14 (^{14}C).

4.1.4. Physico-chemical Parameters

Digital Crison MM 40 and YSI 550A multimeter instruments were used to measure pH, electrical conductivity (EC), temperature, Total Dissolved Solutes (TDS), oxidation reduction potential (REDOX) and dissolved oxygen (DO) measurement readings for the sample waters.

4.1.5. Computer Software

4.1.5.1. Topography

Google Earth Pro and MapInfo Pro software were used to produce a topographic map of the south-eastern region of South Africa which covers the study area. The digital elevation or topography map is a function of Shuttle Radar Topography Mission (SRTM) produced at a 30.6944-meter resolution (Hirt *et al*. 2010).

4.1.5.2. Geochemical Modelling

The pH Reaction Equilibrium Calculation (PHREEQC) geochemical modelling software package (developed by Parkhurst and Appelo, 1999) and Visual MINTEQ v3 geochemical modelling software package (developed by Gustafsson, 2000) were used to carry out speciation in terms of Saturation Indices. The results for the geochemical models were compared with the purpose of improving confidence in using speciation modelling for this study.

Geochemical modelling is a computer-based method of predicting the potential formation of chemical reactions in fluids and mineral precipitations or dissolutions that affect specific biogeochemical environments using simulation models that are based on reaction kinetics and chemical thermodynamics (Zhu and Anderson, 2002; Merkel and Planer-Friedrich 2008; Haase *et al*. 2013).

Geochemical modelling can be sub-categorised into inverse and forward geochemical modelling (Parkhurst and Plummer, 1993; Zhu and Anderson, 2002; Merkel and Planer-Friedrich, 2008). PHREEQC software is the most common freeware used to carry out modelling calculations. Attention was given to speciation modelling (Saturation Indices) since it was the only method used for the present study.

Saturation Index (SI) is defined as a measure of whether mineral phases will dissolve in or precipitate out of solution (Merkel and Planer-Friedrich, 2008; Ledesma-Ruiz *et al*. 2015). In essence, it is the logarithmic proportion of the solubility product (K_{SP}) and ion-activity product (IAP) (Merkel and Planer-Friedrich, 2008; Ledesma-Ruiz *et al*. 2015). Saturation Indices are typically determined from PHREEQC although other alternative software is available and calculates all the SIs for probable mineral phases that can form from available chemical components such as Na^+, Ca^{2+}, HCO_3^-, SO_4^{2-},etc. The purpose of calculating these indices is to determine which phases are either saturated, in equilibrium or undersaturated with respect to the solution in which they are contained (Parkhurst and Appelo, 2012; Ledesma-Ruiz *et al*. 2015). It is, therefore, imperative to determine and characterise the minerals that react or precipitate within the groundwater system (Parkhurst and Appelo, 2012).

4.2. Water-rock Interactions

4.2.1. Stoichiometric Analysis

Stoichiometric analysis is particularly dependent on the usage of major ion concentrations, where concentrations are converted from mg/l into meq/l, which considers mass of an element with respect to concentration (Table 2).

Table 2: Major ion concentrations for the analysed water samples in meq/l.

Sample ID	Ca	Mg	Na	Cl	SO_4	HCO_3
	meq/l					
TC-01	6.94	10.20	41.46	39.32	11.99	13.52

TC-02	16.52	10.86	42.33	37.46	11.97	16.58
TC-03	16.17	10.53	28.71	22.65	6.95	22.50
UM-F	0.39	0.63	0.59	0.35	0.15	1.90
UM-S	14.52	9.95	31.19	29.11	9.22	14.58
UM-U	0.31	0.58	0.40	0.23	0.12	0.89
UM-D	0.34	0.60	0.50	0.28	0.11	0.90
BH-01	2.60	6.33	9.22	6.91	4.46	9.72
BH-02	1.06	2.82	5.74	6.91	0.10	3.54

Hounslow (1995) provided ionic concentration-based ratios (Equations 2 to 5) that can be used to deduce the dominant geochemical processes governing the observed water chemical characteristics. The revised concentrations (in meq/l) for all the analysed water samples are substituted in the ratio expressions.

The dissolution of carbonate and silicate weathering within the aquifer system can be expressed mathematically using Equation 2. Equation 2 is applied to assess the probability of feldspar (i.e. anorthite and albite) silicate weathering. According to Hounslow (1995), its results can be interpreted in a manner such that, if a calculated ratio is < 0.2 or > 0.8, it indicates that there's minimal possibility that plagioclase feldspar weathering took place, whereas a ratio of > 0.2 or < 0.8 signifies a very likely possibility of plagioclase feldspar weathering taking place.

$$\frac{Na^+ + K^+ - Cl^-}{Na^+ + K^+ - Cl^- + Ca^{2+}} \quad (2)$$

The assessment of Ca^{2+} and $SO_4{}^{2-}$ by the ratio in Equation 3 is done with the purpose of determining the provenance of these ions. According to Hounslow (1995), the ratio investigates the possibility of gypsum dissolution, pyrite oxidation and the role of carbonates as the source of freely available Ca^{2+}. The results of this ratio can be interpreted in such a manner that, a ratio of 0.5 is an indication of gypsum dissolution, whereas a ratio of <0.5 accompanied by an acidic pH is an indication of pyrite oxidation (Hounslow, 1995). Moreover, a calculated ratio of <0.5 accompanied by a neutral pH is an indication of calcite precipitation or ion exchange where Ca^{2+} is being removed and lastly, a calculated ratio >0.5 simply implies that carbonates or silicates are the source of Ca^{2+} and not gypsum (Hounslow, 1995).

$$\frac{Ca^{2+}}{Ca^{2+} + {SO_4}^{2-}} \quad (3)$$

Schoeller (1977) proposed that ion exchange can be assessed using chloro-alkaline indices such as CAI-I and CAI-II and states that negative values of the calculated indices serves as an indication of ion exchange between Ca^{2+} moreover, or Mg^{2+} with Na^{2+} in the aquifer system, whereas positive indices values imply that reverse ion exchange is very likely to have occurred. These indices are determined as shown in Equations 4 and 5 below in meq/l.

$$CAI - I = Cl^- - \frac{(Na^+ + K^+)}{Cl^-} \quad (4)$$

$$CAI - II = Cl^- - \frac{(Na^+ + K^+)}{({HCO_3}^- + {SO_4}^{2-} + {CO_3}^{2-} + {NO_3}^-)} \quad (5)$$

These ratios are used as additional tools to assist to build up concise evidence and reach a conclusion on the dominant geochemical processes governing the groundwater system in the study area.

4.2.2. Bivariate Analysis

Bivariate analysis is a statistical method of comparing analysed variables (major ions in this study) with the purpose of determining the correlation between them. A strong correlation/relationship may be an indication of the same source of ions, mineral phases or even process of formation (geochemical processes). The converted major ion concentrations in meq/l are also used for the bivariate analysis.

Kura *et al*. (2013) provide a Guildford's rule of thumb for correlation coefficient classification in Table 3 below.

Table 3: Correlation coefficients classification based on Guildford's rule of thumb (Kura *et al*. 2013).

Correlation coefficient (r-value)	Classification
0.0 – 0.29	Negligible correlation
0.3 – 0.49	Low correlation
0.50 – 0.69	Moderate correlation
0.70 – 0.89	Good correlation
0.90 – 1.00	Best correlation

Chapter 5: Literature Review

5.1. CO_2 Gas Identification in the Study Area

The first interpretation of the natural CO_2 releases from the Bongwana Fault was given by Young (1924) with a focus on Farm Lot 7 (site C on Figure 1-d) and observed that there was CO_2 gas regularly seeping up to the surface – occurring as bubbles in the water of Umzimkulwana River within the vicinity of its western bank. Gevers (1941) added that it was in this exact location where the CO_2 gas bottling plant was built around 1924 with the purpose of exploiting CO_2 gas commercially. The gas bottling plant has since been decommissioned, and the borehole was sealed permanently. On the adjacent neighbouring Farm Lot 10 (site C on Figure 1-d), an approximately 0.6 m-wide N-S trending fault zone is characterised by brecciated and pulverized Dwyka tillite where CO_2 was being released (Young, 1924). The results of samples acquired by Young (1924) gave CO_2 percentages of 98.3% and 97.6% for samples I and II, each one with 0.2% for O_2, whereas for N_2 it was 1.5% and 2.2% by difference for both sample I and II.

5.2. Soil Gas Chemistry and Flux Survey Done in the Study Area

Although the method used by Hicks *et al*. (2014), is not covered in the present study, it is still considered an essential technique for monitoring gas releases along the Bongwana Fault. This forms part of the crucial information that was compiled in the study area by SANEDI and CGS between late 2014 until September 2015. According to Hicks *et al*. (2014), soil gas analyses were performed using steel tube probes of about 4 millimetres internal diameter. The steel probes are hammered into the soil using two steel cylinders that have been welded to the probe tubes, providing hammering surfaces (Hicks *et al*. 2014; Johnson *et al*. 2017).

Hicks *et al*. (2014); Bond *et al*. (2017) and Johnson *et al*. (2017) reported the following results for the soil gas flux survey:

- In Baker's Farm where an area of $36250\ m^2$ was surveyed, the soil was found to have high CO_2 concentrations, half of which were constricted to a narrow approximately 30 metres-wide zone that is trending north. These results were then superimposed to a geological map complied by du Toit (1920), and it was found that the values correspond to a small fault network that was distinctly marked by brecciation in the area. However, due to the establishment of agricultural fields in the area over time, the fault system is now buried and can no longer be seen at the

surface. CO_2 values were found to be decreasing when moving away from the inferred fault network, whereas the plugged CO_2-rich well portrayed fluctuations of the soil concentration values that increased up to 80% CO_2 for two samples taken along the fault line.

- In Umtamvuna, the soil gas flux survey showed a rapid increase in CO_2 gas concentrations in the soil crosswise the fault trace where these CO_2 concentrations can go up 28% with an average flux of 191 $gm^{-2}d^{-1}$ (soil respiration rates units).
- In Manzimhlanga, there had not been any significant variations in the CO_2 gas fluxes in the hillslope soils where the survey was conducted, indicating minimal fluxes owing to the gas exhalation that was first identified in the stream.

5.3. Hydrogeochemical Analysis

The procedure involved measurements of the pH, temperature (℃), electrical conductivity (EC) and dissolved oxygen (DO) besides major ion analysis.

In the Baker's Farm, sampling was conducted on the only two available wells, the CO_2-rich well and the CO_2-poor well (plugged and unplugged) respectively (Hicks *et al*. 2014; Johnson *et al*. 2017). The CO_2-rich well was found to have lower pH (acidic) and elevated electrical conductivity (EC), including higher bicarbonate than the CO_2-poor well, whereas the dissolved oxygen (DO) concentrations also varied significantly between the two wells with the CO_2-rich well having an average of 0.7 mg/l and CO_2-poor well having an average of 2.5 mg/l, respectively (Johnson *et al*., 2017). Moreover, all three samples that were taken and analysed in the water lab, plot as Na-Cl water types as shown by the Piper Plot in Figure 7 (Johnson *et al*. 2017).

In the Umtamvuna area, the waters were found to have electrical conductivity and bicarbonate values that are considerably higher than the Baker's Farm waters (Hicks *et al*., 2014; Hicks, 2015), with similar concentration to the CO_2-rich waters and depleted dissolved oxygen values and lower pH (Figure 8) (Johnson *et al*. 2017).

In Manzimhlanga, stream sampling indicates that there are insignificant variations among the measured parameters such as pH, dissolved oxygen, TDS, alkalinity and major ion analyses owing to groundwater mixing with stream water and small gas fluxes (Johnson *et al*. 2017).

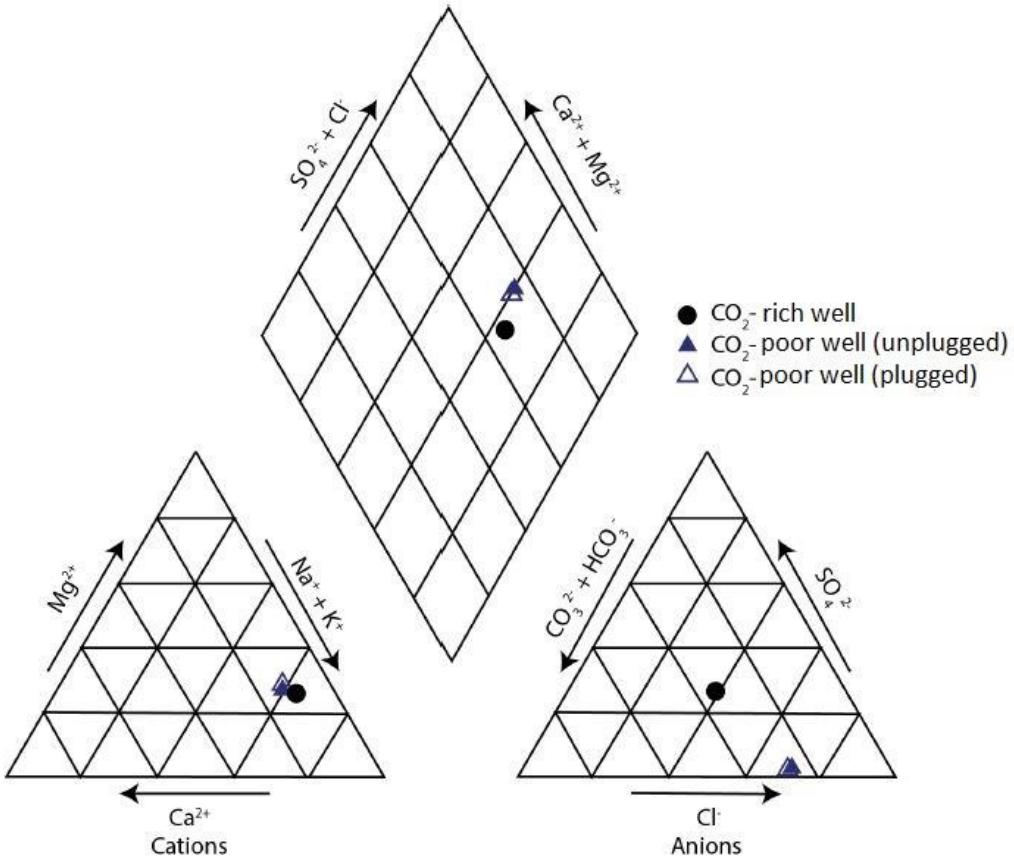

Figure 7: Piper Plot from the Baker's Farm (Source: Johnson *et al*. 2017).

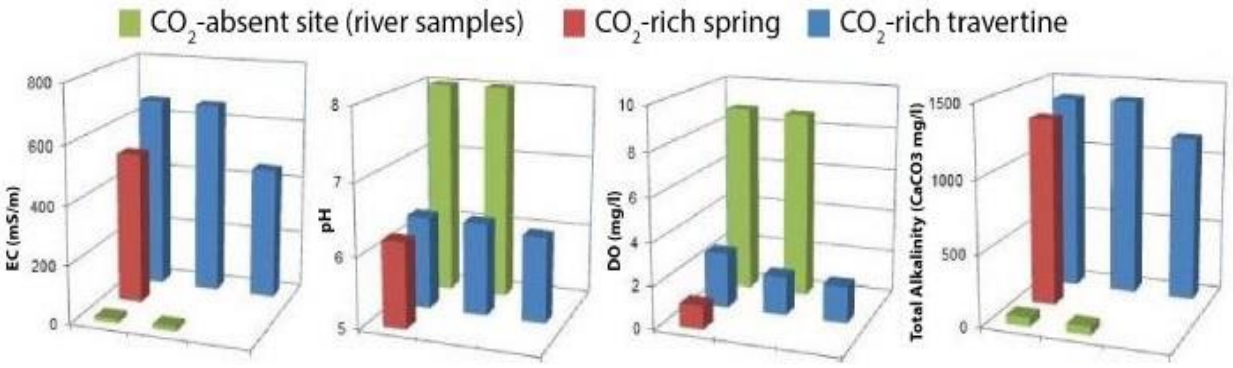

Figure 8: A comparison of physical-chemical variables for CO_2-rich and CO_2-poor sites (a) Baker's Farm, (b) Umtamvuna and (c) Manzimhlanga respectively (Source: Johnson *et al*. 2017).

5.4. Structural Analysis

A well-rounded comprehension of the role that faults and fractures play as fluid pathways is of great importance in order to gather all the necessary information on suitable storage sites that can be used for CCS (Metz *et al*. 2005; Rinaldi and Rutqvist, 2013). It has been previously stated that the biggest threat to the development and implementation of CCS is the negative perception that exist towards unknown adverse effects of leaking CO_2 gas. For this reason, it was imperative to study the role played by fractures and faults as escape pathways for these fluids (Roberts *et al*. 2015).

Hicks *et al*. (2014) utilized the limited fault displacement surfaces in Farm Lot 7 and Lot 10 to map the fault. Furthermore, the acquired orientation and geological information was used to produce a stereonet plot (Figure 9).

Scheiber-Enslin *et al*. (2014) investigated the source of the Beattie magnetic anomaly (BMA) using potential field data and Hicks *et al*. (2014) used these field data to produce an aeromagnetic map of the study area delineating the location of the Bongwana Fault and hence, the approximate location of the CO_2 exhalations (Figure 10).

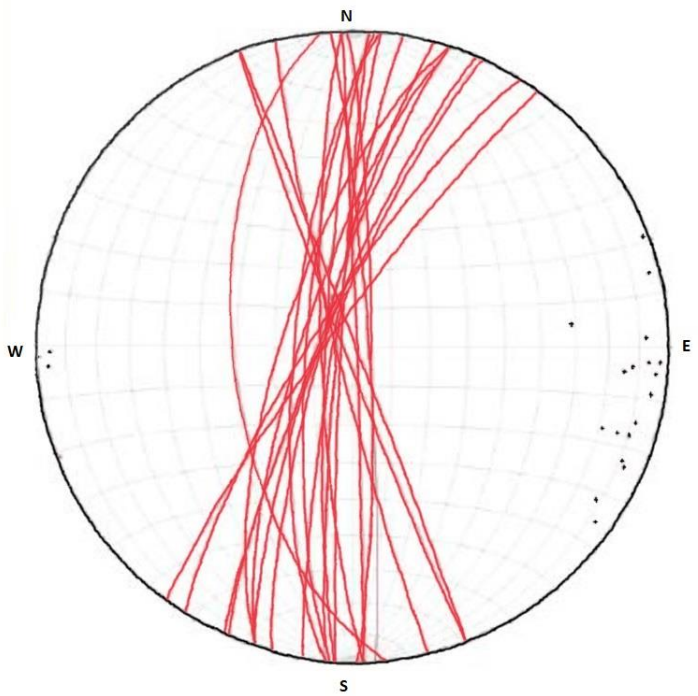

Figure 9: A stereonet plot of the fractures and fault displacement along the Bongwana Fault, showing north-south vertical orientations (Source: Hicks *et al*. 2014).

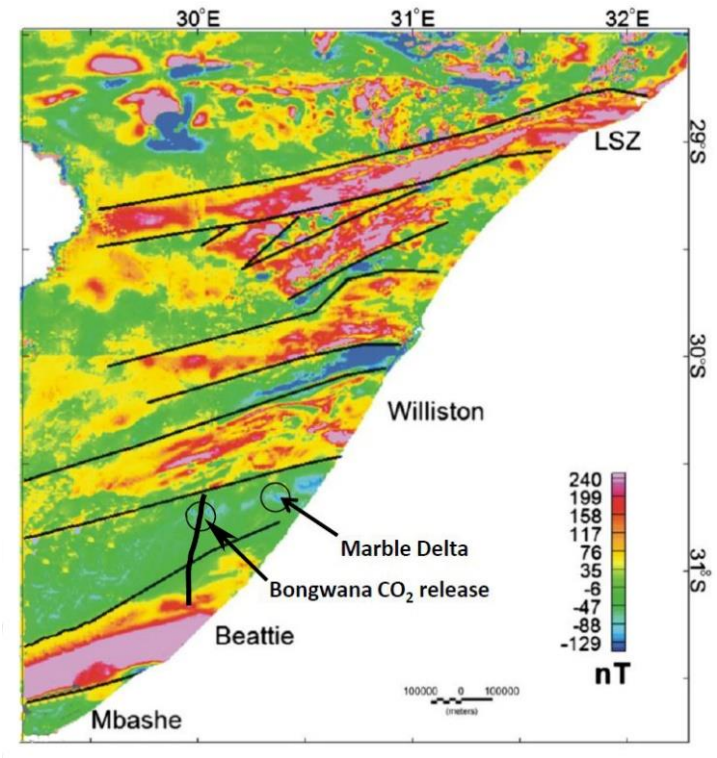

Figure 10: A total magnetic intensity (TMI) image of the south-eastern portion of South Africa showing the Beattie magnetic anomaly (Source: Hicks *et al*. 2014).

A detailed use of aerial photographic techniques with the purpose of ascertaining the measurements of faulting in the study area via the usage of a 3-D virtual outcrop model revealed that there is substantial fracturing along the mapped fault trace (Bond *et al*. 2017). Bond *et al*. (2017) further created hypothetical permeability fracture models based on the acquired geological data and demonstrated the possible scenarios of heterogeneity in fluid flow between the fault/fracture slip surface and the surrounding damage zone, (Figure 11).

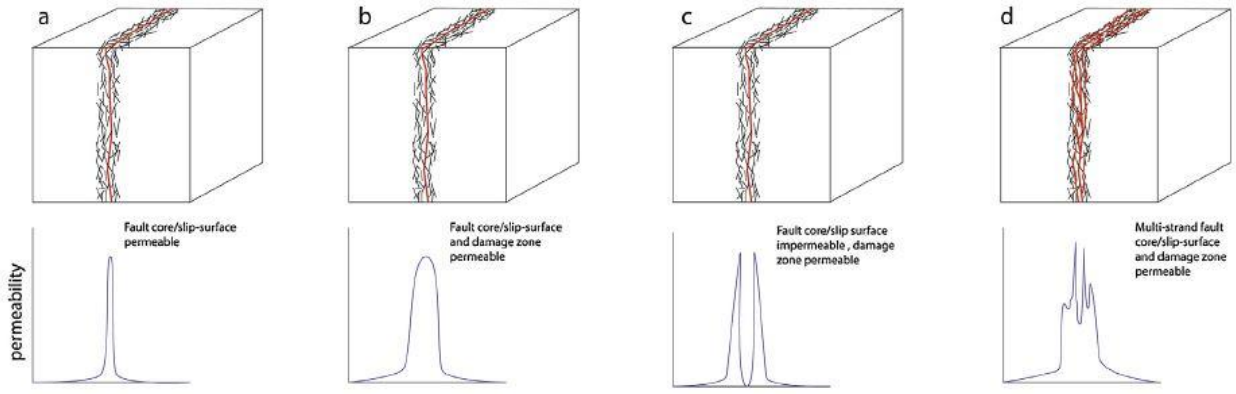

Figure 11: Hypothetical fluid flow model along a fault (Source: Bond *et al*. 2017).

According to Figure 11-a, the fault slip surface (red line) is permeable and allows fluid flow while the surrounding damaged zone is sealed/blind, while Figure 11-b shows the fault slip surface and the surrounding damaged zone are both permeable with increased hydraulic conductivity. Figure 11-c depicts the fault core that is sealed/blind/cemented whereas the surrounding damaged zone is permeable, while in Figure 11-d there is maximum heterogeneity in fluid on the fault core and the surrounding damaged zone.

5.5. Environmental Isotopes

Harris *et al*. (1997) focused more on the carbon isotopes since they can be used to differentiate between marine carbon and mantle-derived carbon. See Table 4 for analytical results.

Table 4: Stable isotope analysis of Bongwana carbon dioxide sampling and Marble Delta carbonates including local groundwater. The $\delta^{18}O$ values are measured relative to SMOW, $\delta^{13}C$ values relative to PDB respectively (Source: Harris *et al*. 1997).

Sample	Location	Sample type	$\delta^{13}C$ (‰)	$\delta^{18}O$ (‰)
1a	Bongwan	CO_2 gas	-0.6	37.3
1b	Bongwan	CO_2 gas	-0.6	38.1
2a	Bongwan	CO_2 gas	-0.5	38.6
2b	Bongwan	CO_2 gas	-0.5	38.4
3	Bongwan	CO_2 gas	0.1	45.1
4	Bongwan	CO_2 gas	-1.0	37.2
5	Bongwan	CO_2 gas	-0.1	37.6
6	Pleasant View	CO_2 gas	0.0	35.3
7	Pleasant View	CO_2 gas	0.9	40.2
MD 1/1	Marble Delta Formation	Carbonate	1.9	24.4
MD 1/2	Marble Delta Formation	Carbonate	1.9	24.3
6	Bongwan	Water	-21 (0.7)	11.4 (0.1)

Harris *et al*. (1997) used the acquired analytical results (Table 4) to compare the Bongwana oxygen and carbon isotope signatures with those of different environments based on the work done by Moore *et al*. (1977), Chacko *et al*. (1991), Doel (1995) and Santo and Clayton (1995) including various models that were proposed. Therefore, the results presented by Harris *et al*. (1997) conclude that the source of CO_2 in the Bongwana Fault is the dissolution of carbonate rocks at depth by acidic groundwater – which attests to the suggestion made by Gevers (1941). Carbonate rocks of the Marble Delta Formation can be seen exposed at the surface about 30 km away eastwards of Bongwana (30°39'21.61"S, 30°20'58.98"E) (Figure 1), and they appear as a folded protolith surrounded by basement lithologies of Meso-Proterozoic ages (Otto, 1973). The presence of these rocks attests to the findings made by Gevers (1941) and hence, subsequently Harris *et al*. (1997).

Chapter 6: Results and Discussion

6.1. Environmental Isotope Analysis

The results of stable isotopes (^{2}H, ^{18}O and ^{13}C) for the groundwater sampled during the field work in October 2017 are presented in Table 5. The results for the stable isotopes of oxygen and hydrogen have been plotted in reference of the Global Meteoric Water Line (Craig, 1961) and Local Meteoric Water Line (Abiye, 2013).

Table 5: Analytical stable isotope results including Cl (mg/L) and calculated deuterium excess (d-excess). The $\delta^{18}O$ values are measured relative to SMOW.

Sample ID	Location	Sample type	$\delta^{18}O$ (‰)	$\delta^{2}H$ (‰)	Cl (mg/L)	d-excess (‰)
BH-01	Baker's Farm (Bongwana)	Borehole water	-5.17	-21.8	245	19.6
BH-02	Baker's Farm (Bongwana)	Borehole water	-5.60	-28.3	245	16.4
TC-01	Umtamvuna (Bizana)	Spring water	-7.49	-22.6	1349	37.4
TC-02	Umtamvuna (Bizana)	Spring water	-7.65	-22.8	1328	38.4
TC-03	Umtamvuna (Bizana)	Spring water	-7.24	-22.5	803	35.4
UM-F	Umtamvuna (Bizana)	River water	-2.52	-9.79	12.4	10.4
UM-S	Umtamvuna (Bizana)	Spring water	-7.9	-22.7	1032	40.5
UM-U	Umtamvuna (Bizana)	River water	-2.85	-9.64	8	13.2
UM-D	Umtamvuna (Bizana)	River water	-2.33	-8.4	10	10.2

Deuterium excess (d-excess) is indicative of an isotope compositional shift from the GMWL and hence, when the $\delta^{18}O$ and $\delta^{2}H$ values are known, d-excess can be determined through a mathematical expression, $d = \delta^{2}H - 8*\delta^{18}O$ (Dansgaard, 1964). In essence, d-excess is a practical way of representing moisture source regions where it can be used to distinguish among possible moisture sources (i.e. the local source of moisture or regional circulation) recharging groundwater in a specific region (Geyh, 2000; Fitts, 2002; Zhu and Anderson, 2002).

The groundwater samples obtained from the study area (TC-01, TC-02, TC-03, UM-S, BH-01 and BH-02) indicate recharge of the aquifer (Msikaba Formation sandstone), with minimal impact from prolonged, regional evaporation rates and hence, are significantly depleted with respect to $\delta^{18}O$ and $\delta^{2}H$ (Figure 12). The Umtamvuna river water samples (UM-F, UM-U and UM-D) are all characterised by relatively warmer in-situ surface temperatures and show significant impact of gradual evaporation rates

by their isotope enrichment relative to groundwater samples and plot within and on both the LMWL and GMWL because of being open to the atmosphere.

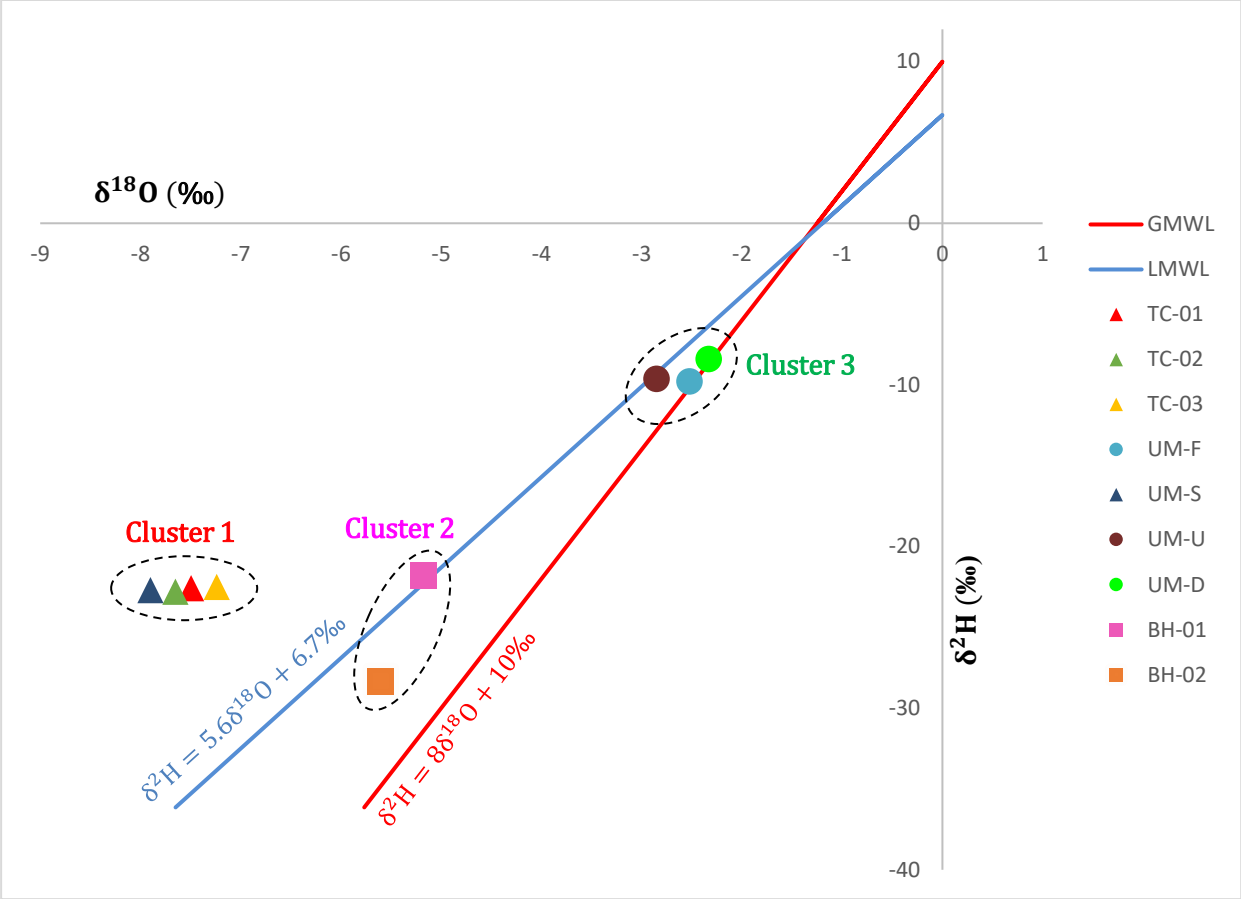

Figure 12: $\delta^{18}O$ vs. $\delta^{2}H$ plot in relation to the GMWL (Craig, 1961) and KZN LMWL (Abiye, 2013).

The groundwater samples collected from the boreholes in Baker's Farm, Bongwana (BH-01 and BH-02) plot close to the LMWL (cluster 2). This indicates the significant influence that local rainfall has on these waters. The analysis indicated that the measured isotopic composition of this water (BH-02) is depleted with respect to the environmental isotopes and this can be interpreted as groundwater with a deeper circulation at colder temperatures (Figure 12). Deep circulation of groundwater recharged during cold weather results in isotopic depletion.

Water samples from Umtamvuna travertine cones and spring (TC-01, TC-02, TC-03 and UM-S) all plot above the local meteoric water line. The isotope plot (cluster 1) indicates CO_2 exchange and that the deeply circulating water interacts with the carbonates (Figure 12). The isotopic compositions of the Umtamvuna springs samples (TC-01, TC-02, TC-03 and UM-S) are clustered close to one another,

indicating a possible connection via a fracture network at depth since the travertine cones and the spring are situated within very close proximity to one another.

When looking at the deuterium excess (Table 5), water samples from Umtamvuna have higher d-excess (35.4‰, 37.3‰, 38.4‰ and 40.5‰) whereas the water samples from Bongwana area have lower d-excess (16.5‰ and 19.6‰). This indicates that the possible source of moisture for the water recharging the Umtamvuna springs could be local, whereas rainfall related to a regional circulation recharges in Bongwana. The Umtamvuna river water samples are characterized by the lowest d-excess (10.2‰, 10.4‰ and 13.2‰), indicating water originating from a regional circulation. This makes sense since Umtamvuna River receives tributaries that get water from a wider catchment.

When looking at the chlorine concentrations compared against the $\delta^{18}O$ values, water samples from Umtamvuna springs are more enriched in Cl concentrations (803 mg/l, 1032 mg/l, 1328 mg/l and 1349 mg/l) as compared to water samples from Bongwana (both having 245 mg/l). Umtamvuna river water samples have the lowest Cl concentrations (8 mg/l, 10 mg/l and 12.4 mg/l) and this makes sense for a fresh river water (see Table 5 and Figure 13). Higher chlorine concentration in groundwater usually indicate the impact of higher evaporation rates in shallow aquifers or evaporitic minerals acting as sources of chlorine via leaching from the surrounding rocks (water-rock interactions).

The isotopic trends in Figure 12 indicate that the meteoric water has very little to no influence when it comes to recharging the groundwater seeping up to the surface from the Umtamvuna springs. Hence, the only possible logical explanation is that the recharge water probably comes from older waters (coastal groundwater) at depth or brackish/sea water intrusion into the Msikaba Formation sandstone, which is the aquifer in this region. Meteoric water can also be ruled out as a possible source of recharge again based on elevated salinity detected in these waters. The salinity, electrical conductivity and TDS measurements classify the Umtamvuna springs water as brackish water (coastal groundwater). This is possible since Umtamvuna is situated very close to the sea (Figure 16).

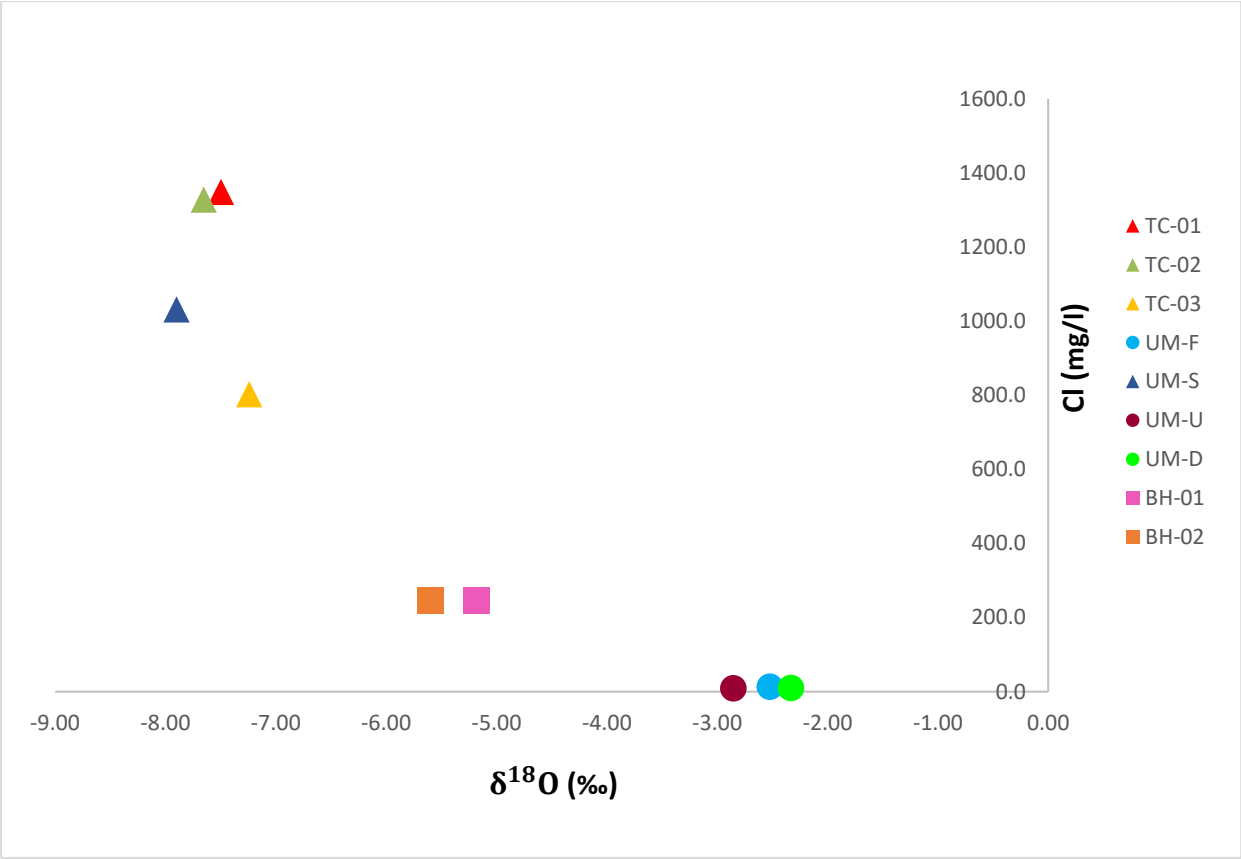

Figure 13: A comparison of $\delta^{18}O$ against Cl concentrations for the analysed water samples.

Note that the above plot (Figure 13) shows a sort of exponential decrease in Cl as 18-O value increases that can support the source of chloride from rocks and soil horizon than evaporation.

However, the Bongwana water samples (BH-01 and BH-02) isotopic signatures indicate recharge by precipitation rich in chloride (or recharge into marine palaeo-groundwater with higher chlorine levels), typical of rainfall that is not far from the sea (Figure 14). Bongwana and Umtamvuna are separated by ~15 km, whereas Umtamvuna is situated the closest to the sea (~36 km inland) when compared to Bongwana (~57 km inland).

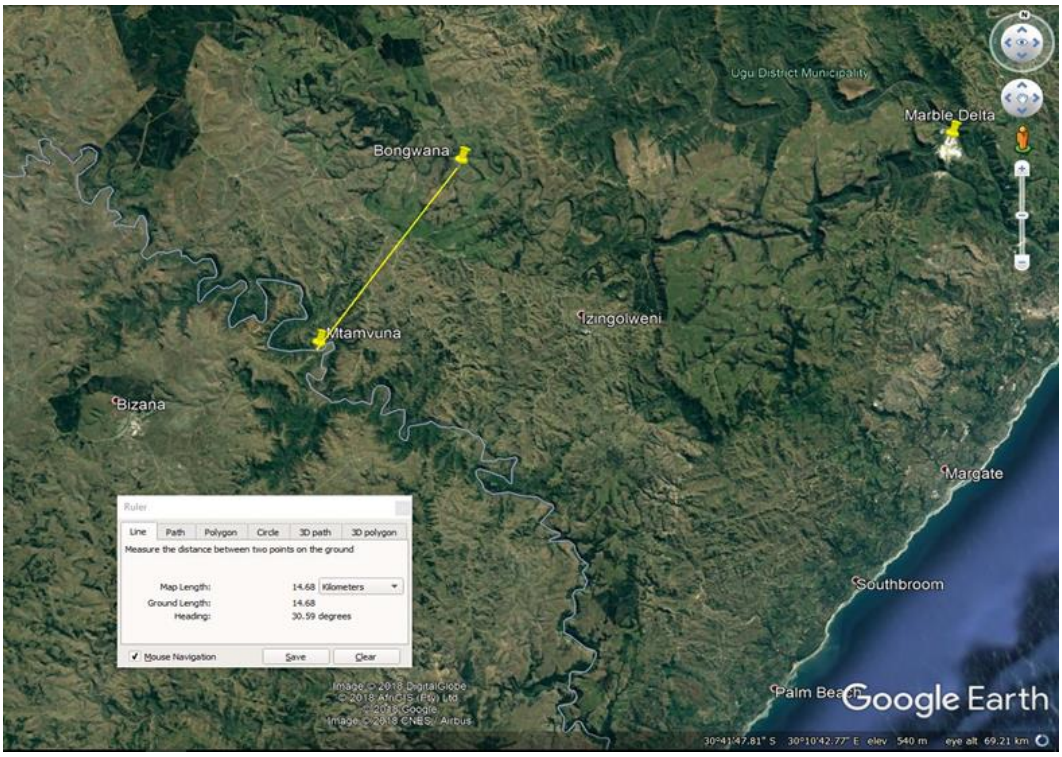

Figure 14: Google Earth relative locations of Bongwana and Umtamvuna. Notice the Marble Delta carbonate quarries on the NE section of the image (pinned).

Table 6: Results for the stable isotope of carbon ($\delta^{13}C$).

Sample ID	Sample Type	$\delta^{13}C$ (‰ PDB)
BH-01	Borehole water	-1.69
BH-02	Borehole water	-1.47
TC-01	Spring water	1.56
TC-02	Spring water	1.55

When it comes to the carbon-13, only water samples were considered and not CO_2 gas and travertine fragments around the Umtamvuna cone springs.

The water samples from Bongwana sampling area were characterised by a depleted $\delta^{13}C$ value of -1.69 and -1.47‰ whereas the Umtamvuna waters had relatively enriched $\delta^{13}C$ values of +1.55 and +1.56‰ respectively, see Table 5. These values concur with the isotopic values, i.e., -0.6 to +0.9‰ presented in Table 3 where Harris *et al*. (1997) correlated with carbon originating from carbonate rocks as initially proposed by Gevers (1941) rather than a mantle magmatic source as proposed by Hartnardy (1985). Hence, these results confirm that the CO_2 detected in the groundwaters of the study area originate from the reaction of acidic groundwater with carbonates at depth.

Sampling points for this study are different from the sampling points of the study conducted by Harris *et al*. (1997) within the same study area. The comparative plot in Figure 15 indicate that the isotopes in the study area are not distributed equally. In essence, there is significant isotope differentiation.

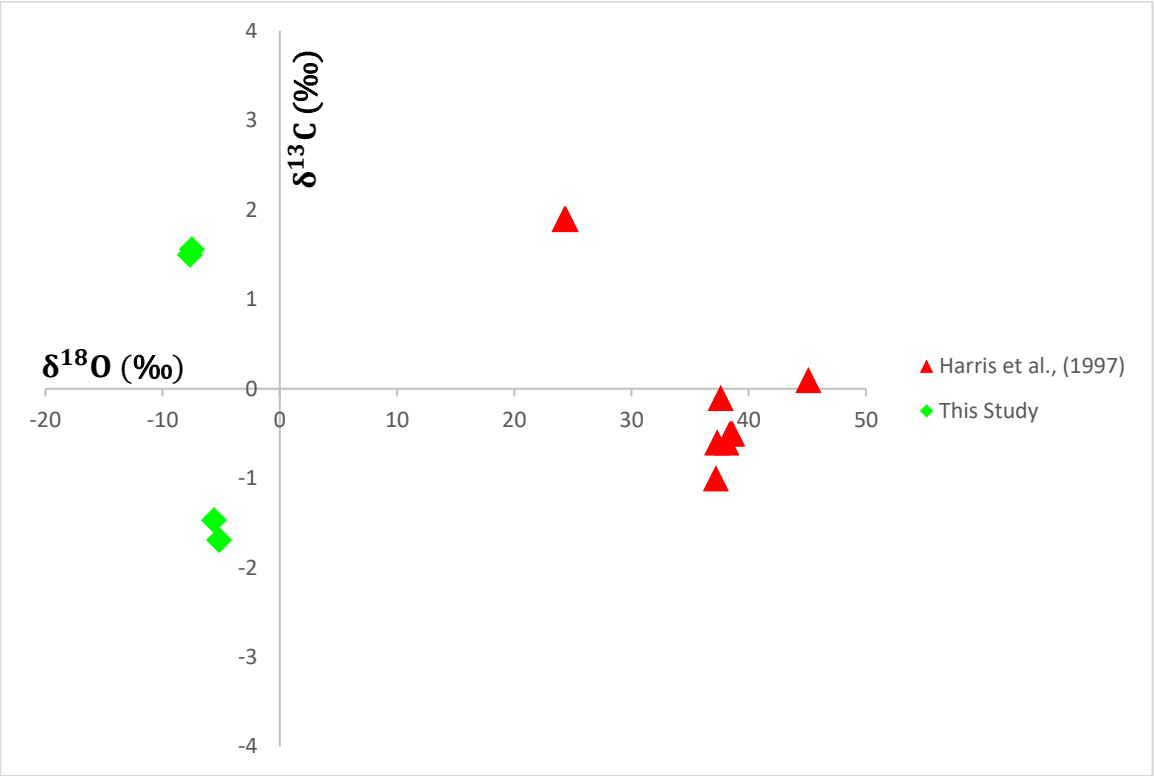

Figure 15: Comparison of isotopic compositions between this study and Harris *et al*., (1997) for deducing the CO_2 source along the Bongwana Fault.

Carbonate rocks of marine or sedimentary origin are characterised by $\delta^{13}C$ values ranging from close to 0 to +2‰ while the CO_2 of magmatic origin has relatively depleted $\delta^{13}C$ values of approximately -6‰ (Schoelle and Arthur 1980; Geyh, 2000; Hiscock, 2005; Clark and Fritz, 1997 and Ryan, 2014). Hence, the similarities between the literature and the measured $\delta^{13}C$ values confirm the proposition of a sedimentary-marine carbonate source for the CO_2 emitting in the Bongwana Fault.

In Bongwana, there are no exposed travertines at surface or springs available, but water samples were collected from boreholes drilled within the agricultural fields (Baker's Farm). The carbonates occur probably at a depth where the groundwater would react to produce the CO_2 intersected by the borehole (BH-01). The BH-01 water sample gave a depleted $\delta^{13}C$ value of -1.69‰ and the possible reason for this depletion might be attributed to CO_2 uptake by plants for photosynthesis since there are agricultural fields in the area that might be absorbing carbon from the soils.

Ehleringer *et al*. (1993) stated that the sensitivity and the uptake of carbon-13 by plants is dependent on the availability of moisture and hence, $\delta^{13}C$ can also be used to trace variations in environmental precipitation. The $\delta^{13}C$ depletion is prevalent in the study area because of the presence of agricultural fields. Geyh (2000) also stated that soils are characterised by $\delta^{13}C$ values of -22 to -11‰ and plants are most depleted with -30 to -20‰, whereas the evaporitic carbonate minerals tend to be isotopically enriched with up to +10‰.

Plotting of the Bongwana Fault groundwater isotopic compositions within the travertine field (Figure 16) also gives an idea of how different environments through which carbonates precipitate or dissolves relate to one another, in particular, the influence of a marine environment on the groundwater compositions of the study area. This is clear as it is supported by elevated chlorine levels detected in the groundwater (Figure 13) and by the proximity of the study area to the sea (Figure 14). The position of groundwater from the study area within the travertine field also agrees with actual field observations of the travertine mound and cone springs (Figures 2.1 – 2.3). The groundwater of the study area dissolves and carries the Marble Delta Formation carbonate material and isotopic composition signatures to the surface.

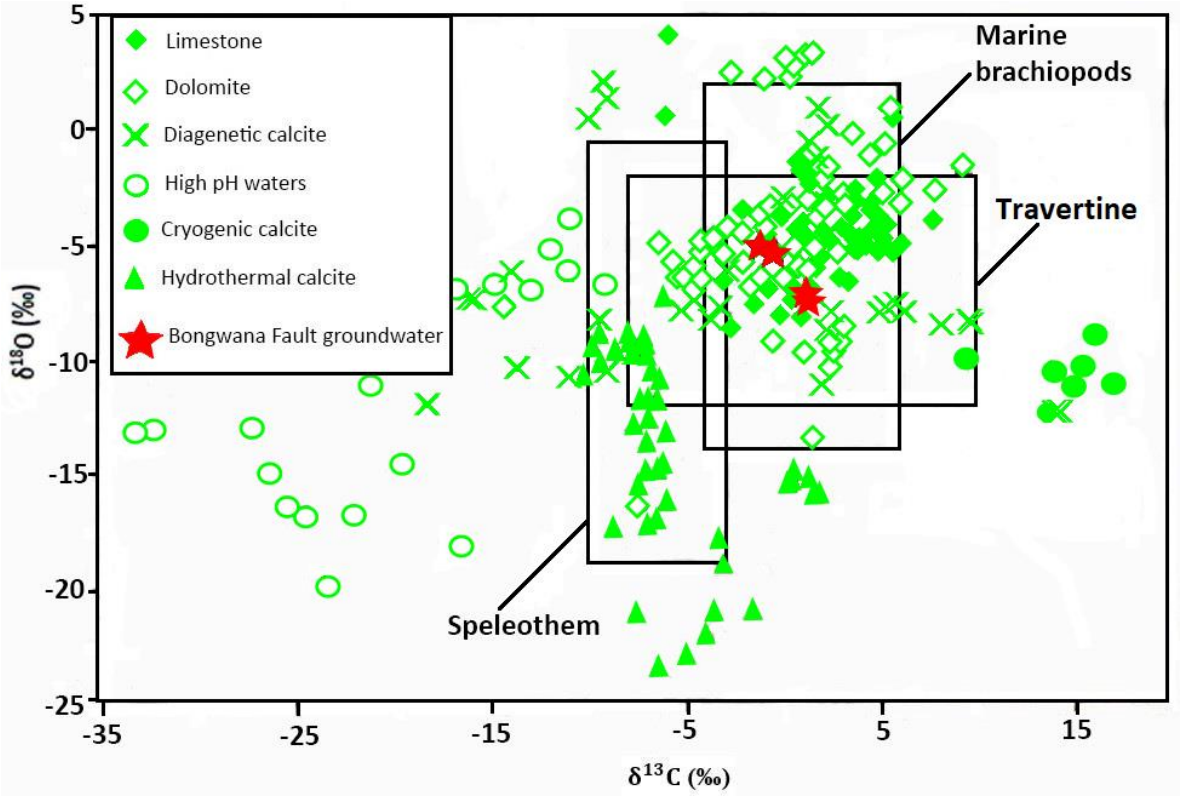

Figure 16: A comparison of $\delta^{18}O$ and $\delta^{13}C$ compositions from this study with literature (Source: Clark and Fritz, 1997).

6.1.1. Radiogenic Isotopes Analysis

The results for the radiogenic isotopes (^{3}H and ^{14}C) for the groundwater sampled during field work in October 2017 are given in Table 7.

Table 7: Radiogenic isotope results with the mean ^{14}C Mean Residual Time.

			MRT
Sample ID	**$\delta^{13}C$ (‰ PDB)**	**^{14}C (pMC)**	**^{14}C (years)**
BH-01	-1.69	1.5 ± 1.6	$34\,718 \pm 50$
BH-02	-1.47	1.2 ± 1.4	$36\,504 \pm 50$
TC-01	1.56	0.0 ± 1.5	$50\,000 \pm 50$
TC-02	1.55	0.0 ± 1.5	$50\,000 \pm 50$

MRT: Mean Residual Time

In regard to carbon-14, mean residual time of water was determined based on the Dissolved Inorganic Carbon (DIC) content which entered the groundwater via the soil zone from the atmospheric $^{14}CO_2$. From Table 7, it can be noted that these groundwater samples are characterised by "dead" carbon ratios attributed to the Marble Delta Formation carbonate dissolution at depth and precipitation of travertine at surface (observed in Umtamvuna).

Clark and Fritz (1997); Pentecost (2005) gave the decay equation through which mean residual time can be calculated and it is as follows:

$$t = -8267 * \ln \frac{a_t{}^{14}C_{DIC}}{q * a_0{}^{14}C} \quad (6)$$

$a_0{}^{14}C$ is the initial carbon-14 value with $a^{14}C_{DIC}$ being the measured carbon-14 from tritium-bearing groundwater. Therefore, the stipulated radiocarbon ages for the DIC in the groundwater of the study area determined in Table 7 are calculated as follows:

E.g., for sample BH-01

$$t = -8267 * \ln \frac{1.5\ pMC}{100\ pMC} \quad (7)$$

$$= \mathbf{34718.96\ years}$$

The 100 pMC for the $a_0{}^{14}C$ used is the modern pre-nuclear bombing atmospheric levels related to the 1950 Anno Domini's 13.56 dpm/g carbon.

The calculated radiocarbon ages imply that the carbonate has been dissolving to give off the CO_2 detected in the groundwater of the study area for at least ~34, 700 years BP for the Baker's Farm water samples and at least ~50, 000 years BP for the Umtamvuna water samples. However, the recrystallisation of calcite to form the travertine mound and cones seen in Umtamvuna (Figures 2.1 – 2.3) is a later and hence, younger process. Radiogenic carbon is a function of time, and its amount decreases in rocks as they become older (Fitts, 2002).

In general, what this implies is that, the groundwater from the study area is relatively younger, but carries an older carbon (DIC) signature due to its interaction with the marble from the Marble Delta Formation at depth. Moreover, the calculated carbon-14 mean residual times give an estimate of roughly how long the geochemical processes responsible for the CO_2 exhalations detected in the study area have been dominant.

6. 2. Hydrogeochemistry

6.2.1. Physico-chemical Analysis

The physico-chemical parameter measurements collected in the field are presented in Table 8.

Table 8: Physico-chemical parameters measured in the study area.

Sample Code	Physico-chemical parameters				
	pH	**T (℃)**	**EC (mS/m)**	**DO (mg/l)**	**Field observations**
TC-01	5.80	21.1	650	1.8	There was a smell of sulphur in the spring.
TC-02	6.00	21.8	650	3.03	There were algae present along the mouth of the spring.
TC-03	5.80	21.7	413	2.54	This spring bubbles less than the TC-01 and TC-02 springs.
UM-F	6.60	25.3	10.5	6.57	River sampling done along the fault trace.
UM-S	5.90	21.3	525	3.35	Spring is often flooded during heavy rainfall periods.
UM-U	7.71	25.3	9.7	7.93	Sampling done upstream.
UM-D	7.72	25.7	9.9	8.95	Sampling done downstream.
BH-01	5.25	23.0	124.7	1.6	Borehole was poorly cased and abandoned.
BH-02	5.98	23.2	81.8	0.8	Borehole did not encounter carbon dioxide unlike BH-01.

Temperature

The water samples reflect the average temperatures of their surroundings and these temperatures are relatively constant due to insulation, averaging 21.5 ℃ for the Umtamvuna groundwater samples and 23.1℃ for Bongwana groundwater samples. Moreover, the Umtamvuna River has an average temperature of 25.7℃ reflecting the surroundings surface temperatures.

The temperatures, i.e. 21.5 ℃ for the Umtamvuna groundwater, 23.1℃ for Bongwana groundwater and 25.7℃ for Umtamvuna River, are relatively average especially when taking the Umtamvuna travertine springs into consideration (Figures 2.1 – 2.3). This is as compared to other well-known examples of travertine deposits such as the Appalachians thermal springs characterized by temperatures reaching up to 84℃ attributed to the presence of a magmatic heat source (Hobba *et al*. 1979) and the European cryogenic cave carbonates which precipitated under freezing temperatures (~0℃), see Zak *et al*. (2012). In Bongwana not much can be said as far as temperature is concerned since there are no travertines or any carbonates exposed at surface; the water sampled from the boreholes only reflects the average

temperatures of the surroundings. The presence of these travertine surfaces and cones in Umtamvuna triggered an interest around the investigation of factors which contributed to their deposition.

Total Dissolved Solids (TDS)

For this study, TDS was determined in the lab during major ion analyses at 180℃ by dry boiling (Table 9). This parameter is crucial in the sense that it helps with water classification as it increases with salinity. All the Umtamvuna groundwater samples are classified as brackish (moderately saline) water with TDS >1000 mg/l (ranging from 3356 to 4500 mg/l), whereas Bongwana groundwater samples fall under fresh water classification, their TDS is still >500 mg/l (ranging from 573 to 856 mg/l), which indicates the influence of salinity in the regional coastal aquifer system in the area. The Umtamvuna river is classified as freshwater with TDS<1000 mg/l (ranging from 155 to 173 mg/l) and it makes sense since Umtamvuna river get its water from various streams forming tributaries taking their water from afar sources (Figure 17-a).

In general, TDS is high for CO_2-rich waters and relatively low for the CO_2-poor waters – a trend that was also noted by Johnson *et al*. (2017) for the same area.

Electrical Conductivity (EC)

The CO_2-rich waters are characterised by high EC, averaging 124.7 mS/m in Bongwana and ranging from 413 to 650 mS/m in Umtamvuna, with an average of 559.5 mS/m. The CO_2-poor waters have relatively low EC values ranging from 9.7 to 10.5 mS/m with an average of 10.03 mS/m for the Umtamvuna River water and 81.8 for Bongwana.

Dissolved Oxygen (DO) and pH

DO as a measure of the highest oxygen concentration that can dissolve in water, is inversely proportional to salinity and impacts greatly on water quality since it controls the solubility of various trace metals and serves as a biological indicator (Weaver *et al*., 2007). The DO values range from 0.6 mg/l for CO_2-rich waters to 8.95 mg/l for CO_2-poor waters (Table 8). This is consistent with the salinity trend that is high for the CO_2-rich waters. CO_2 is formed by the consumption of any free oxygen available and hence, CO_2-rich waters are characterised by relatively low DO values. The great depth at which the CO_2-rich waters come from also contributes to their low DO nature. The Umtamvuna River which is classified as freshwater is therefore characterised by relatively higher DO values due to its interaction with the atmosphere (Figure 17-c).

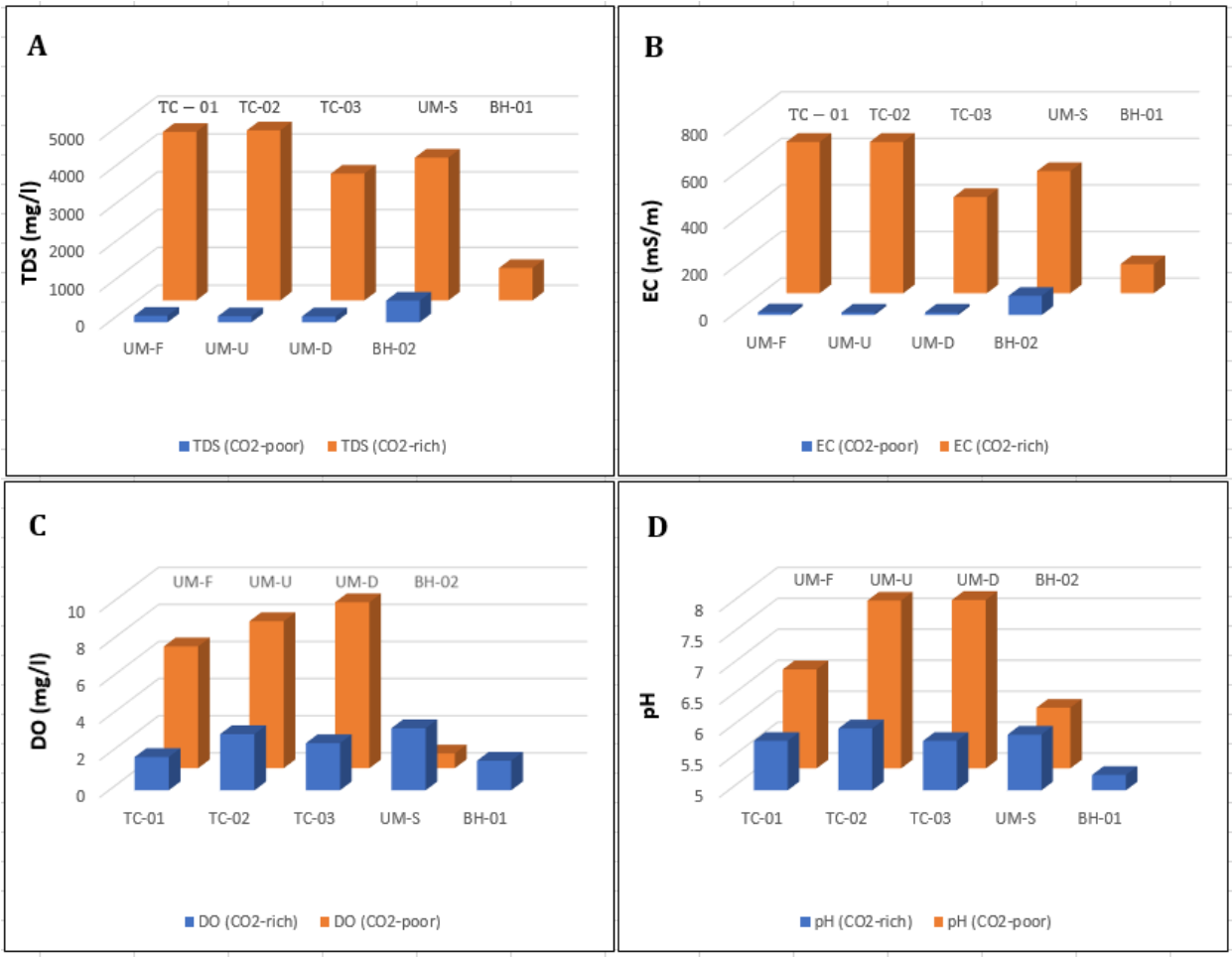

Figure 17: A comparison of different physico-chemical parameters for CO_2-rich waters against CO_2-poor waters; (a) Lab TDS, (b) EC, (c) DO and (d) pH.

The in-situ results for pH measurements confirm that carbonates (calcite) dissolves and gives off CO_2 which becomes a dominant species in water, and is stable at pH <7 (average 5.75 for CO_2-rich waters). The CO_2(aq) phase is not in equilibrium with the surroundings and is subjected to chemical transformation when pH is buffered (pH ~ 6 – 8) due to consistent degassing, bicarbonate (HCO_3^-) then becomes a dominant species. This statement holds true since HCO_3^- for the groundwater samples ranges from 215.94 mg/l in Bongwana and up to 1372.5 mg/l in Umtamvuna when the temperature is raised to 25°C (Table 9).

The pH ranged from 5.25 to 6.0 for the CO_2-rich waters and 6.60 to 7.72 for the CO_2-poor waters at an average temperature of 23.2°C (Table 8). These results show that the CO_2-rich waters are characterised by the highest concentrations of HCO_3^- and shift towards CO_3^{2-} as pH continues to rise (Figures 18).

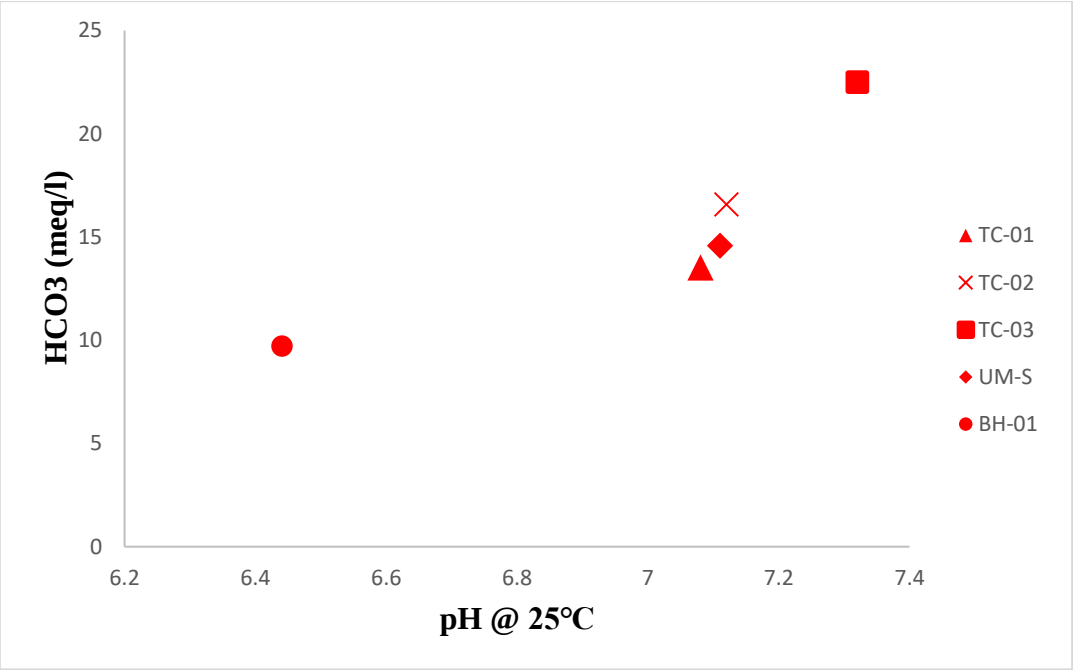

Figure 18: pH vs HCO_3 for the analysed CO_2-rich waters of the study area.

6.2.2. Hydrochemical Analysis

The overall order abundance for major ions is as follows, $Na^+ > Ca^{2+} > Mg^{2+} > Fe^{2+}$ for cations of all the water samples and $Cl^- > {HCO_3}^- > {SO_4}^{2-}$ for samples TC-01, TC-02 and UM-S, whereas ${HCO_3}^- > Cl^- > {SO_4}^{2-}$ for samples TC-03, UM-F, UM-U and UM-D as far as anions are concerned (Table 9).

Table 9: Major ion analyses results for the analysed water samples of the study area

Date sampled		12-Jul-17	12-Jul-17	12-Jul-17	12-Jul-17	12-Jul-17	12-Jul-17	12-Jul-17	12-Jul-17	12-Jul-17
Sample type		Water	Water	Water	Water	Water	Water	Water	Water	Water
Locality description		TC-01	TC-02	TC-03	UM-F	UM-S	UM-U	UM-D	BH-01	BH-02
Analyses	Unit									
Field pH	pH	5.80	6.00	5.80	6.60	5.90	7.71	7.72	5.25	5.98
Lab pH	pH	7.08	7.12	7.32	7.86	7.11	8.19	8.21	6.44	7.11
EC @ 25℃	mS/m	662	673	468	15.3	581	14.2	14.4	160	106
TDS @ 180℃	mg/l	4040	4292	2984	122	3460	108	118	1130	526
HCO_3	mg/l	824.72	1011.4	1372.5	66.37	889.38	54.05	54.66	592.92	215.94
Cl	mg/l	1349	1328	803	12.4	1032	8.31	9.79	245	245
SO_4	mg/l	576	575	334	7.02	443	5.82	5.49	214	4.96
NO_3-N	mg/l	0.89	0.917	0.915	1.11	0.951	1.08	1.06	0.934	1.25
B	mg/l	0.950	2.18	0.949	<0.013	1.04	<0.013	<0.013	0.137	<0.013
NH_4-N	mg/l	1.07	1.24	0.967	0.079	0.957	0.072	0.074	0.654	2.07

F	mg/l	4.64	4.26	3.26	<0.263	4.75	<0.263	<0.263	0.517	0.699
Ca	mg/l	139	331	324	7.76	291	6.24	6.89	52.2	21.2
Mg	mg/l	124	132	128	7.6	121	7.02	7.34	77	34.3
Na	mg/l	953	973	660	13,5	717	9.18	11,4	212	132
Fe	mg/l	<0.04	<0.04	<0.04	<0.04	<0.04	<0.04	<0.04	9.12	<0.004
Mn	mg/l	0.009	0.419	0.633	<0.001	0.486	<0.001	<0.001	0.84	0.156
Total hardness	mg as $CaCO_3$/l	858	1369	1337	51	1224	44	47	448	194
DO	mg/l	2.94	4.52	2.32	5.52	2.1	6.45	5.92	0.7	1.6

In general, Na^+ and Cl^- are the dominant ions with the HCO_3^- levels are also high due to the interaction with the carbonate source at depth and hence, mixing processes of different anion end members can occasionally lead to cases where $HCO_3^- > Cl^-$ as seen with sample TC-03 characterised by 1372.5 mg/l for HCO_3^- while the Cl^- is 803 mg/l for the same sample (Figures 19 and 20). The issue with stream samples (UM-F, UM-U and UM-D) is that the Umtamvuna stream collects fresh water and subsequently dilutes the unique chemical compositions of the waters from the study area. Hence, samples show a variation in the salinity concentrations in comparison with the groundwater samples. Moreover, due to their little to no CO_2, their alkalinity and sulphate concentrations also show this variation.

There is a general variation in the SO_4^{2-} concentration among CO_2-rich waters (TC-01, TC-02, TC-03, UM-S and BH-01) and CO_2-poor waters (UM-F, UM-S, UM-D and BH-02) with an average concentration of 428.40 mg/l and 5.82 mg/l, respectively.

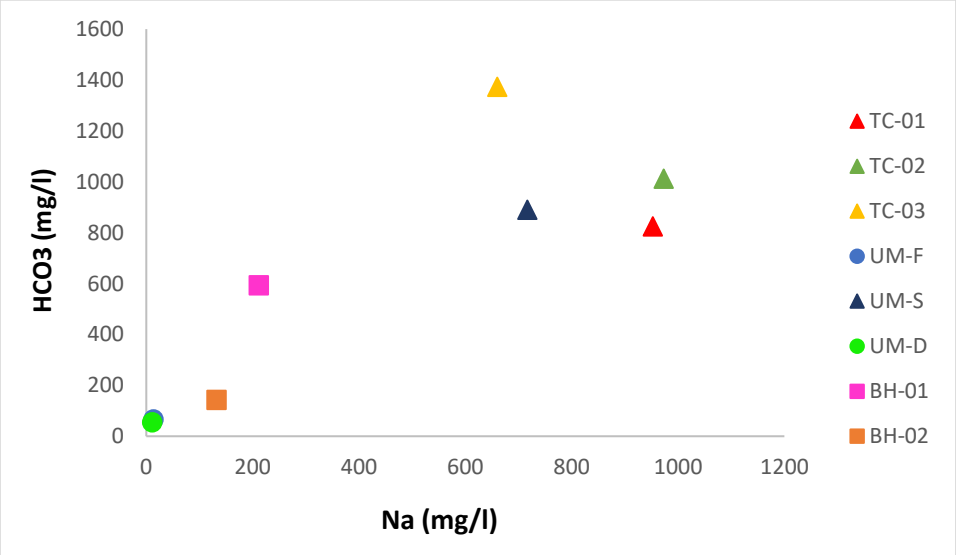

Figure 19-a: Binary plot of Na and HCO_3.

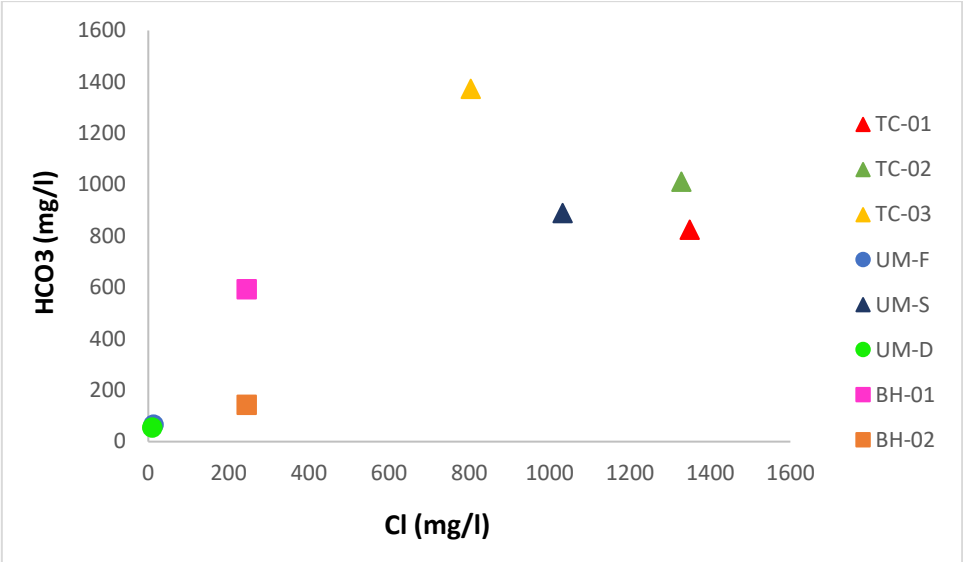

Figure 19-b: Binary plot of Cl and HCO_3.

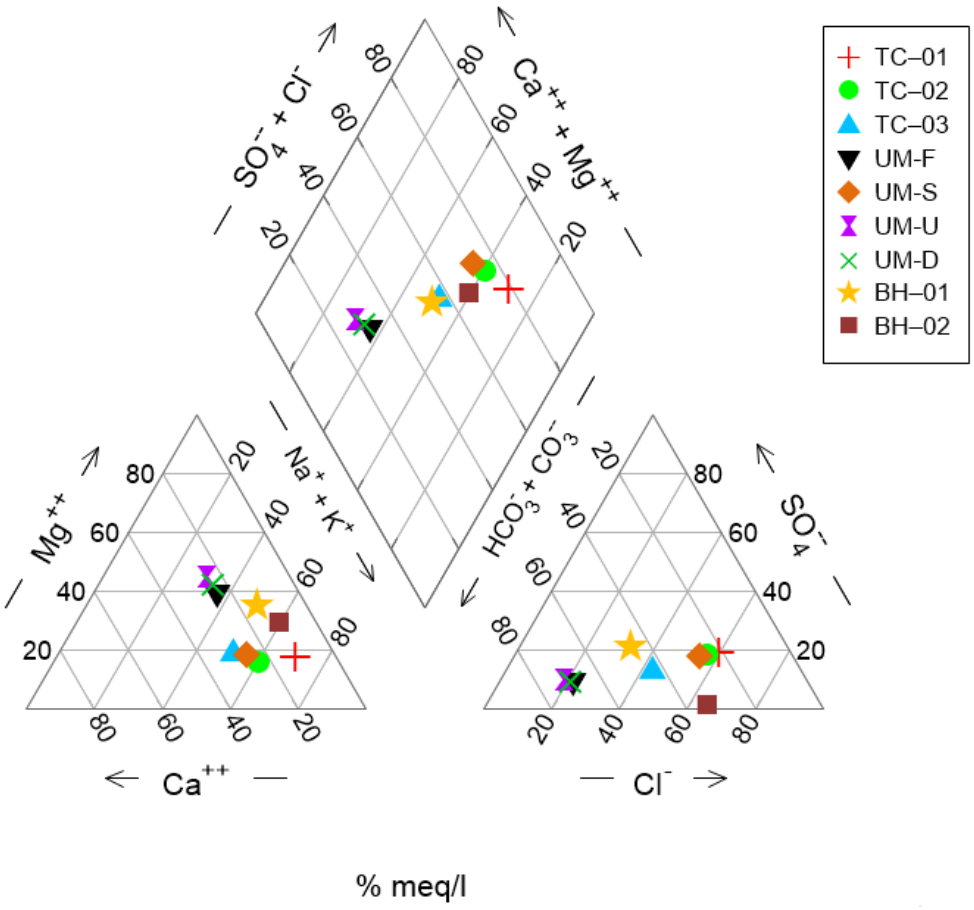

Figure 20-a: Piper plot for the samples in the study area.

The Piper Plot in Figure 20-a indicates that the water samples analysed are from different sources as indicated by varying water chemistries.

Based on the Piper Plot (Figure 20-a), the hydrochemical facies observed are presented in Table 10.

Table 10: Bongwana Fault water types

Sample ID	Sample location	Resultant water type
TC-01	Umtamvuna	Na-Cl-HCO_3-SO_4
TC-02	Umtamvuna	Na-Ca-Cl-HCO_3-SO_4
TC-03	Umtamvuna	Na-Ca-Cl-HCO_3
UM-F	Umtamvuna	Mg-Na-Ca-HCO_3-Cl
UM-S	Umtamvuna	Na-Ca-Cl-HCO_3
UM-U	Umtamvuna	Mg-Na-Ca-HCO_3
UM-D	Umtamvuna	Mg-Na-Ca-HCO_3-Cl
BH-01	Bongwana	Na-Mg-HCO_3-Cl
BH-02	Bongwana	Na-Mg-Cl-HCO_3

The Na-Ca-Cl-HCO_3 facies is dominant in the discharge areas, indicating that the chemical evolutionary trend is mostly attributed to hydrochemical mixing. The Mg-Na-Ca-HCO_3-Cl facies of the Umtamvuna River are assumed to be recently recharge water with strong relation to the atmospheric precipitation. The Na-Mg-HCO_3-Cl could have evolved from the interaction of Ca-Mg-HCO_3 and Na-Cl.

The plot in Figure 20-a also indicates that the Umtamvuna river water samples UM-F, UM-U and UM-D along with Bongwana borehole water sample BH-01 are mixed. Umtamvuna water sample TC-03 also mixes unlike all other springs (TC-01, TC-02 and UM-S) that relate to it in close proximity.

The Durov plot on Figure 20-b shows that the analysed water samples plot along the “dissolution or mixing line” and trend towards “reverse ion exchange” indicating that reverse ion exchange, dissolution and water mixing are the dominant geochemical processes as compared to ion exchange. Water samples from an open system such as the Umtamvuna stream samples would be expected to be dominated by “mixing” as evidently shown previously by isotope results and major ion analyses results whereas the groundwater samples would be dominated by a combination of dissolution predominantly and mixing on a minor degree including ion exchange which controls the Na-Cl concentrations.

The pH and TDS (mg/l) are also included on this expanded graphical representation, but they will not be discussed further as they were already discussed in greater detail in Section 6.2.1.

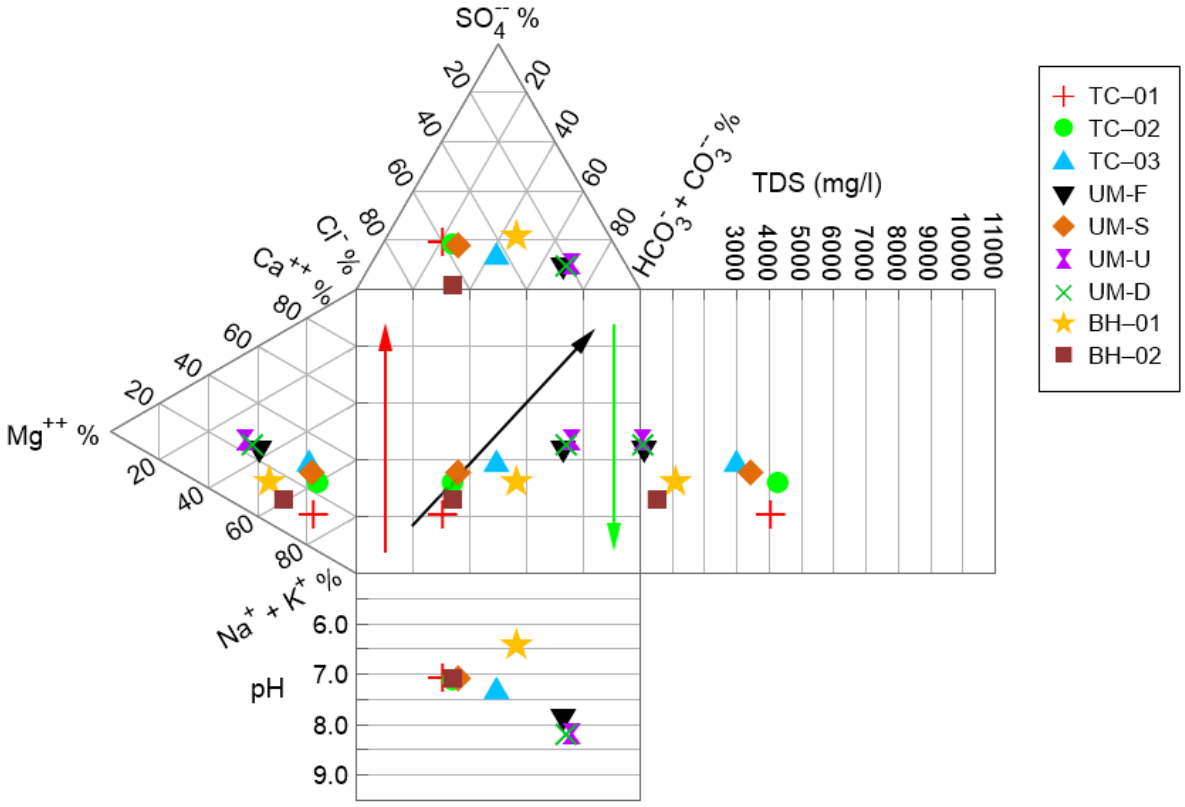

Figure 20-b: Durov plot. The red arrow represents "ion exchange", the black arrow represent "simple dissolution or mixing" and the green arrow represent reverse ion exchange respectively.

The chloro-alkaline indices (CAI) as per the Equations 4 and 5, provide a good insight regarding the exchange of ions between the water and host rock. Based on the analogy explained in Section 3.2.1 all the groundwater samples (TC-01, TC-02, TC-03, UM-S, BH-01 and BH-02) gave positive CAI ratios (CAI-I > 0 and CAI-II > 0) (Table 11). This indicates that the aquifer system is dominated by reverse ion exchange under the influence of either connate waters or simply coastal aquifer groundwater where Ca and Mg ions in the aquifer matrices are exchanged for Na (see the water facies in Table 10).

Schoeller classification in Figure 20-c graphically represents the order of major abundances per water sample. Sample BH-02 is characterised by the lowest concentration (in meq/l) of SO_4 – a significant variation when compared to the BH-01 concentration of SO_4 since the two boreholes are situated near each other (~320 m apart).

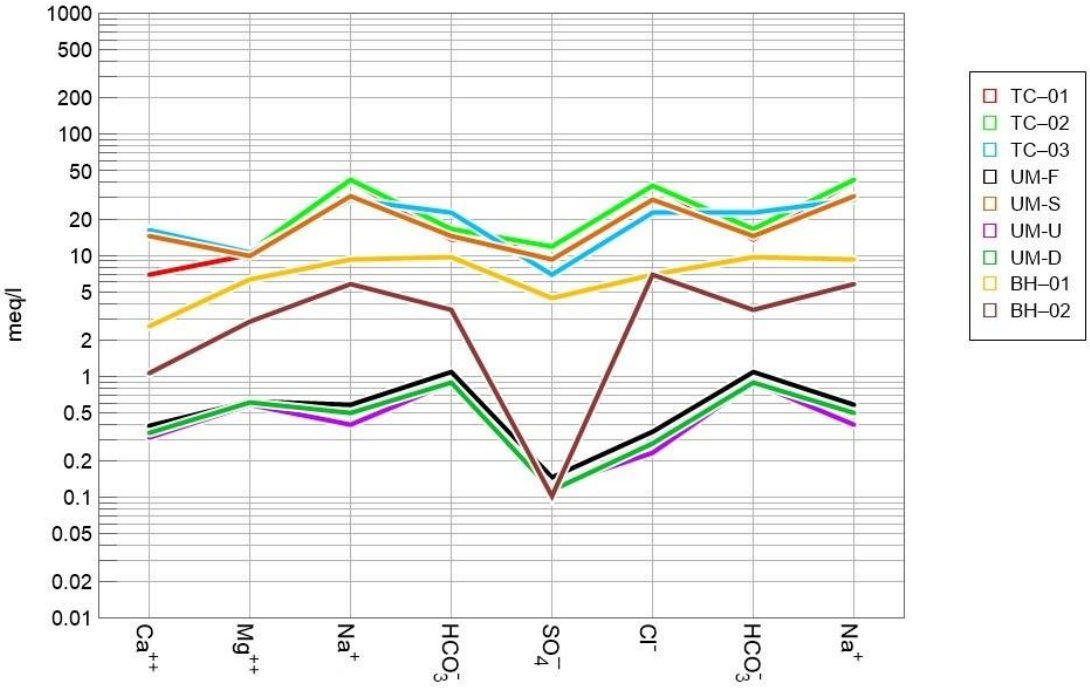

Figure 20-c: Schoeller plot classification of the analysed water samples for the Bongwana Fault study area.

Probable chemical reactions that could be governing the water major ionic compositions are discussed in this section. These reactions are indicated as Equations 8 - 12.

6.2.2.1. Carbonate Dissolution

Carbonate dissolution is triggered by the reaction of carbonate rocks at depth with acidic groundwater and hence, it became imperative to understand how the groundwater of the study area came to be acidic. According to Nolan (1962), the presence of excessive dissolved iron in ferrous form (Fe^{2+}) in groundwater is the main source of groundwater acidity at pH levels below 7. Groundwater in the study area can become enriched in iron by leaching the surrounding Fe-bearing rocks and minerals such as hematite that Thomas and Otto (1991) stated that it is present and is amalgamated with the dolomite marble in minor proportions.

Therefore, a proposition is made that the acidification of the groundwater in the study area occurred in the following steps:

- Available reduced ferrous iron reacts with ambient excess carbon dioxide to form ferrous bicarbonate as represented by Equation 8.

$$FeO\ (aq) + 2CO_2\ (aq) + H_2O\ (l) \rightarrow FeH_2(CO_3)_2\ (aq) \quad (8)$$

- The carbon dioxide embedded in ferrous bicarbonate upon being exposed to the open atmosphere as the water seeps to the surface, then degasses to facilitate the precipitation ferric hydroxide as represented by Equation 9.

$$4FeH_2(CO_3)_2\ (aq) + 10H_2O\ (l) + O_2\ (g) \rightarrow 4Fe(OH)_3\ (s) + 8H_2CO_3\ (aq) \quad (9)$$

Equations 8 and 9 give and support logical explanations for the following observations in the study area:

- There is an oxidation of ferrous iron to ferric iron, appearing as iron hydroxide insoluble precipitate that is seen as "iron rust staining" around the mouth of the travertine springs in Figures 2.1 and 2.2.
- Furthermore, the precipitation of this ferric hydroxide could be the reason why there is very low dissolved ferrous iron detected in the major iron analysis results (Table 9). This implies that, ferrous iron is being consumed to form ferric hydroxide.
- Equation 9 shows that as more ferric hydroxide forms, there is carbonic acid (hence acidic groundwater) that forms as a by-product. This is the same carbonic acid that continues to drive the sub-surface carbonate dissolution process represented by Equation 10 below.

The presence of large quantities of CO_2 detected in the groundwater of the study area via degassing further provides evidence for carbonate dissolution and dissolution process can be expressed by Equations 10 and 11 as given by Earle (2015), Equation 10 when it is calcite dissolving.

$$CaCO_3\ (s) + H_2CO_3\ (l) \leftrightarrow Ca^{2+}\ (aq) + 2HCO_3^-\ (aq) \quad (10)$$

Carbonate dissolution process can be expressed by Equation 11 when it is dolomite dissolving

$$CaMg(CO_3)_2\ (s) + 2H_2CO_3\ (l) \rightarrow Ca^{2+}\ (aq) + Mg^{2+}\ (aq) + 4HCO_3^-\ (aq) \quad (11)$$

The above equations imply that carbonates at depth react with slightly acidic groundwater to dissolve and result in elevated CO_2 detected in the groundwater at pH <7 accompanied by in-situ lower temperatures, whereas at relatively higher room temperature (≥25℃) with pH ≥7, HCO_3^- dominates and hence it can be detected in high quantities in Table 9. Rau *et al*. (2001) suggested that although Equations 10 and 11 are more specific to the alkalinity and hence, the alkaline groundwater solutions formed will still comprise substantial CO_2 because of being in chemical equilibrium with the DIC

carbonate system, which in turn result in carbonate precipitation in the form of travertine as the CO_2 gets into contact with the atmosphere.

The presence of extensive travertine cone and mound springs in the study area (Figures 2.1 – 2.3) reflects geochemical and biochemical processes controlling the carbonate system within since carbonate precipitation is controlled by the pCO_2, pH and the water temperatures at which precipitation was induced. Umtamvuna springs are relatively cool with temperatures around 20 – 23℃, unlike other well-known travertine deposits which are hosted in hot springs with temperatures >30℃.

Christiansen (2001); Pentecost (2005) and Liu *et al*. (2012) stated that travertine deposits form in the following manner:

- Temperature plays a crucial role since a heat source at depth heats the supersaturated groundwater at elevated pCO_2 conditions.
- Upon reaching the surface of the spring, the CO_2 dissolved in groundwater at lower pH conditions degasses as a result of coming into contact with the relatively lower atmospheric pCO_2, thereby increasing the pH to form supersaturated alkaline waters.
- Precipitation is then induced, and as the process iterates, the carbonate precipitate will accumulate along the preferential flow paths and the mouths of the springs forming the cones and mounds seen in Figures 2.1 – 2.3.
- Any surficial process such as evaporation, et cetera leading to the reduction of pCO_2 encourages more travertine to form for as long as there are carbonates available to dissolve at depth.
- Both aragonite and calcite being polymorph end-members of $CaCO_3$ form in these travertine springs, but the most significant difference between them is that, calcite is favoured at relatively lower temperatures whereas aragonite precipitates at higher temperatures.

Liu *et al*. (2012) stated that travertine is marked distinctly by three stages of precipitation and evolution: (i) precipitation and depositional period, (ii) the formation of travertine cone period and (iii) the demise period. The travertine in Figures 2.2 and 2.3 represents the cone formation stage, and then later follows the demise stage as it stops growing.

The springs in the study area are situated in the Dwyka tillite of the Karoo Supergroup, whereas the Marble Delta Formation carbonates which are now assumed to be the source of CO_2 in the area, predates the Karoo. The process of formation of these travertines raises a question regarding the source of heat which produced them since a volcanic source has been ruled out based on the acquired and analysed evidence. Thomas and Otto (1991) discussed various metamorphic processes such as contact

metamorphism and low-temperature retrograde metamorphism which dominated the Marble Delta Formation and could have provided the much-needed heat source to produce these travertines.

The process of travertine formation is intertwined directly with carbonate dissolution in the form of reversible chemical reactions (Equation 10). Pentecost (2005) and Liu *et al*. (2012) described the formation of travertine using Equation 12.

$$Ca^{2+}\,(aq) + 2HCO_3^{-}\,(aq) \leftrightarrow H_2O\,(l) + CO_2\,(g)\uparrow + CaCO_3\,(s)\downarrow \qquad (12)$$

Equation 12 indicates that carbonates interact with acidic groundwater at depth and dissolves until the groundwater solution is supersaturated, and upon reaching the surface, CO_2 dissolved in water forms bubbles as it degasses, leaving behind a travertine precipitate.

6.2.2.2. Silicate Weathering

The process of silicate weathering happens at a very slow rate when compared to other processes such as carbonate dissolution due to reaction kinetics. As such, it subsequently takes longer to notice its influence in the groundwater chemistry (Appelo and Postma, 2005). Goldich (1938); Walraevens *et al*. (2007) discussed the hierarchy of silicate minerals in terms of their weathering rates. These authors stated that plagioclase feldspar is the first silicate to weather with very high potential of influencing the groundwater chemistry, followed by micas particularly biotite, then muscovite – in that order, whereas quartz is the last silicate mineral to weather owing to its high resistance. Liu *et al*. (2011) add that the breakdown of these silicate minerals leads to the formation of clay minerals such as montmorillonite or kaolinite depending on the available favourable conditions. Similar to carbonate dissolution, elevated concentrations of Ca^{2+}, Na^{+}, K^{+} and SiO_2 ions in groundwater can serve as evidence that silicate dissolution took place in the groundwater system (Walraevens *et al*. 2007; Liu *et al*., 2011). Ferro-magnesian silicates are not discussed in this study owing to the fact that iron was found to be present in negligible amounts of <0.04 mg/l for all samples (Table 9). The reason for these low concentrations is given by Equations 8 and 9.

The probability of silicate weathering was investigated using the stoichiometric ratios in Equation 4 and 5 in Section 3.2.1. The calculated ratios of >0.2 or <0.8 indicate silicate weathering according to Equation 2. Hence, the results indicate that all the analysed water samples except sample BH-02 which did not encounter CO_2 at depth have ratios >0.2 and <0.8. This could serve as an indication that there is plagioclase feldspar weathering in the study area (Table 11). This statement holds true since there is

extensive kaolinite clay mineral associated with tillite leaching by CO_2-rich groundwater along the Bongwana Fault. Based on the studies by Paige-Green (1980); Thomas and Otto (1991) and Hicks *et al*. (2014), the dominant plagioclase minerals in the study area are anorthite (Equation 13) and albite (Equation 14).

Equation 13 demonstrates a reaction with acidic (CO_2-rich) groundwater to form kaolinite (Hounslow, 1995; Clark, 2015).

$$CaAl_2Si_2O_8\ (s) + 2H_2CO_3\ (l) + H_2O\ (l) \rightarrow Al_2Si_2O_5(OH)_4\ (s) + Ca^{2+}\ (aq) + 2HCO_3^-\ (aq) \quad (13)$$

Appelo and Postma (2005) and Clark (2015) stated that albite weathering is characterized by relatively less HCO_3^- when compared to that of anorthite. Equation 14, given by Appelo and Postma (2005) is a demonstration of albite weathering to montmorillonite.

$$3NaAlSi_3O_8\ (s) + H_2O\ (l) + Mg^{2+}\ (aq) \rightarrow 2Na_{0.5}(Al_{1.5}Mg_{0.5})Si_4O_{10}(OH)_4\ (s) + 2Na^+\ (aq) + H_4SiO_4 \quad (14)$$

Montmorillonite and kaolinite are the clay mineral phases that are most likely to form from plagioclase feldspar weathering. Appelo and Postma (2005) indicated that montmorillonite is favoured in regions characterised by prolonged drier periods of low rainfall, whereas kaolinite form in sub- to humid and subtropical regions. This could be the case in the study area, as it is situated in the eastern region of Southern Africa where the climate is relatively humid and subtropical, where kaolinization distinctly marks the fault zone.

6.2.2.3. Water-rock interaction ratio calculations

The results presented in Table 11 are calculated based on the conversions presented in Table 2 and Equations 2 to 5 as well as individual cations and anions.

Table 11: Water-rock interactions calculations for the analysed samples.

Sample ID	$\frac{Na}{Cl}$	$\frac{Ca}{Mg}$	$\frac{Ca}{Ca + SO_4}$	$\frac{Ca + Mg}{HCO_3}$	$\frac{Na + K - Cl}{Na + K - Cl + Ca}$	CAI-I	CAI-II
	meq/L						
TC-01	1.05	0.68	0.37	1.27	0.24	38.27	37.70
TC-02	1.13	1.52	0.58	1.65	0.23	36.33	35.98

TC-03	1.27	1.54	0.70	1.19	0.27	21.39	21.68
UM-F	1.69	0.62	0.72	0.54	0.38	-1.33	-0.12
UM-S	1.07	1.46	0.61	1.68	0.23	28.04	27.80
UM-U	1.74	0.53	0.72	1.00	0.35	-1.47	-0.16
UM-D	1.79	0.57	0.76	0.94	0.39	-1.52	-0.21
BH-01	1.33	0.41	0.37	0.92	0.47	5.58	6.26
BH-02	0.83	0.38	0.91	1.10	0.64	6.08	5.34

6.2.2.4. Bivariate Analysis

Bivariate correlations were employed with the purpose of investigating the relations between cations and anions and hence, determining the source of reactions responsible for the dominant mineral phases in the study area. Moreover, it was designed to assist in ascertaining the information based on the dominant geochemical reactions in the study area.

The correlation plots (Figure 21-a – 21-f) were plotted to identify the dominant geochemical processes and for the demonstration of the relationship between the cations and anions (correlation coefficients). Good correlations are indicative of ions that evolved from the same or similar mineral phases and hence, closely-related geochemical processes.

The correlation coefficient results in Table 12 indicate a general good-to-best correlation between the analysed ionic concentrations with the exception of Ca-SO_4 interaction. These classifications are based on Table 3 in Section 3.2.2.

Table 12: A representation of correlation coefficients (r) for the bivariate plot analysis

Bivariate plot	Correlation coefficient (r-value)
Ca vs HCO_3	0.86
HCO_3 vs Ca + Mg	0.92
Ca vs Mg	0.80
Na vs Cl	0.99
Ca vs SO_4	0.67
Mg vs SO_4	0.89

6.2.2.4.1. Calcium vs HCO_3

Ca and HCO_3 sourced from calcite dissolution in the aquifer system allow the analysed samples to plot along the 1:2 ratio line according to Garrels and Mackenzie (1971) as stated in Section 3.4.2, whereas Ca-Mg and HCO_3 sourced from dolomite allow the analysed samples to plot along the 1:4 ratio line. Figure 21-a indicates that there was no sample that plotted on the dolomite ratio, with sample BH-01 plotting on the calcite ratio. A majority of other samples are dispersed within the diagram indicating a mixture of Ca and Mg from different sources. Spring samples and the boreholes samples were of interest since the stream samples have small overall concentrations which do not give any meaning in this regard, hence they plotted very close to the origin. The calcium and bicarbonate as shown in Table 12 has very good correlation (0.86), indicating that they both formed under the same geochemical process, carbonate dissolution, which is assumed to be the dominant process in this study.

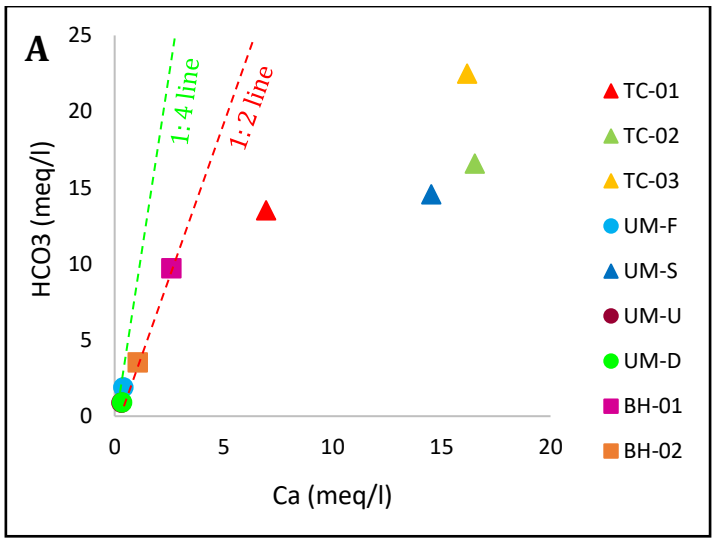

Figure 21-a: Ca vs HCO_3 bivariate plot for the analysed water samples.

6.2.2.4.2. HCO_3 vs Calcium + Magnesium

Based on the analogy explained in Section 3.2.2, both Ca and Mg have the best correlation with HCO_3 (Table 12), serving as an indication that they are all from the same source. The calcium carbonate mineral phases found within the study area were accompanied by high Mg concentrations (Figure 21-b). The calculated ratios in Table 11 indicate that the stream samples UM-F, UM-U and UM-D including borehole sample BH-01 are characterised by ratios ≤ 1 as a result of influence of recent rainfall recharge on the chemical compositions of these waters. The springs samples TC-01, TC-02, TC-03 and UM-S comprise calculated ratios >1. These findings authenticate the stable isotope findings in Section 6.1.

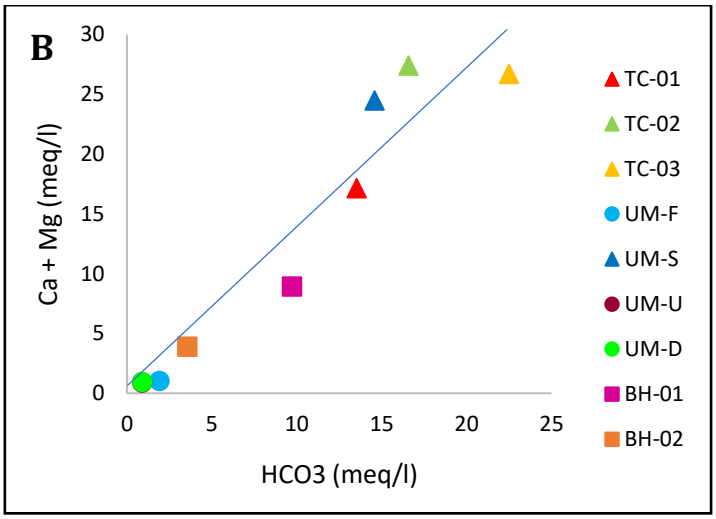

Figure 21-b: HCO_3 vs Ca + Mg bivariate plot for the analysed water samples.

6.2.2.4.3. Sodium vs Chloride

The Na vs Cl scatter plot was done (Figure 21-c) and it resulted in an excellent correlation of 0.99 (Table 12) and hence, all the analysed samples plot directly along the 1:1 equiline (halite dissolution line). This indicates that Na and Cl are coupled together to form halite which is dissolved and as such, it is thus assumed that halite dissolution could be the main source of salinity in the water of the study area. High salinity is typical of coastal aquifers and in regions characterised by high evaporation rates (Ferguson and Gleeson, 2012).

All the samples are more enriched in Cl than Na, which Jalali (2007) and Ferguson and Gleeson (2012) attributed to reverse ion exchange which could have exchanged Na and Ca in the solution and also, the mixing of fossil water with recent recharge water in the aquifer, or even a combination of both processes. When looking at where all the samples have plotted with respect to the 1:1 equiline (Figure 21-c), it can be assumed that the salinity in the study area is governed by a combination of both processes although the influence of recent recharge waters is relatively small particularly for the spring water samples.

The results further indicate that the salinity in the spring waters has no significant influence towards the stream water and hence, the wide variation in the measured Na and Cl concentrations between the springs, boreholes and the stream samples. For this reason, the stream sample concentrations plot very close to the origin as freshwater end member. The calculated ratios for Na/Cl are fairly variable, ranging from 0.83 to 1.79 with an average ratio of 1.32 (Table 11). Ratios >1 facilitate the possibility of other sources or processes other than halite dissolution that can also release Na into the solution; sodic plagioclase weathering if it is present in significant concentrations for example (Meyback, 1987; Rajmohan and Elango, 2004).

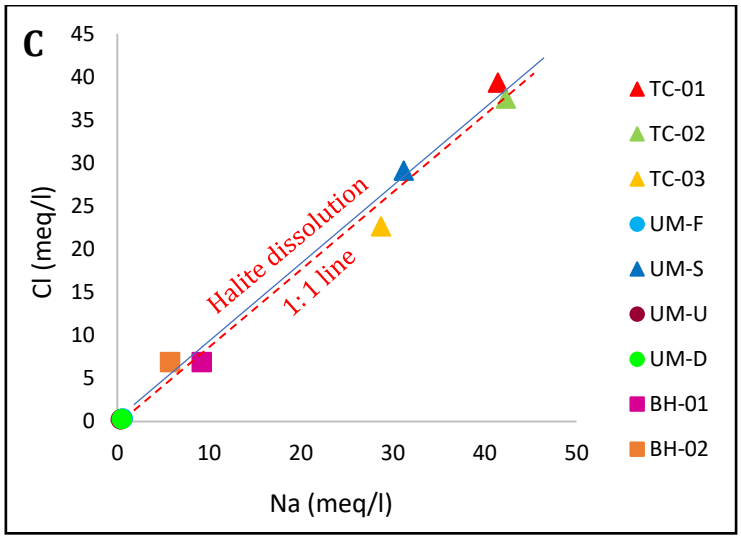

Figure 21-c: Na vs Cl bivariate plot for the analysed water samples.

6.2.2.4.4. Calcium vs Sulphate

The Ca vs SO_4 scatter plot in Figure 21-d gave a moderately good correlation of 0.67 (Table 12). It is thus a likely possibility that some of the calcium in water was sourced from the same process as sulphate, for example: via gypsum dissolution contributing to the water salinity similar to halite, attributed to ion exchange that could have occurred. All the analysed samples are distributed unevenly, few below (BH-02 and TC-03) and a majority above the 1:1 equiline (TC-01, TC-02, UM-S and BH-01). Samples that show more sulphate enrichment relative to calcium plot above the 1:1 equiline, whereas the opposite is true in a situation where calcium is more enriched comparable to sulphate. Jalali (2007) states samples will plot directly on the 1:1 equiline if gypsum is the likely source of freely available Ca and SO_4 in water.

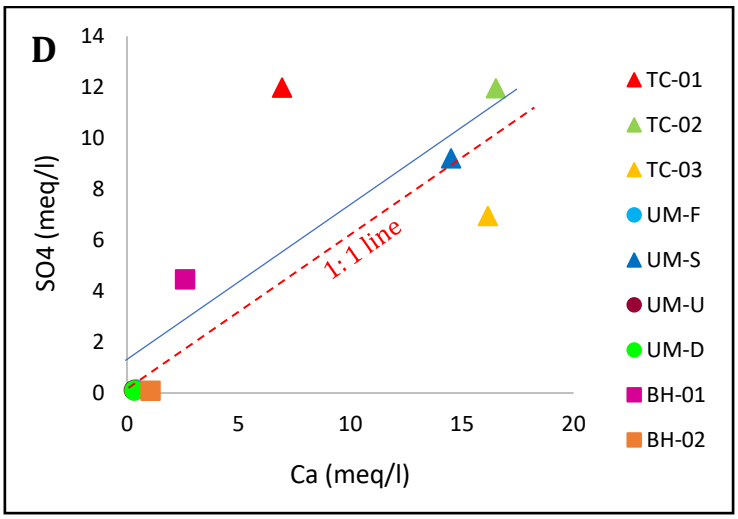

Figure 21-d: Ca vs SO_4 bivariate plot for the analysed water samples.

6.2.2.4.5. Magnesium vs Sulphate

The Mg vs SO_4 scatter plot in Figure 21-e gave a very good correlation of 0.89 (Table 12) indicating a very close relation between Mg and SO_4, although most of the Mg occur in association with Ca and HCO_3 in this study. Fitts (2002) and Steiger *et al*. (2011) stated that dissolved Mg-SO_4 ions in the form of salts such as epsomite ($MgSO_4.7H_2O$) are the second highest source of salinity in sea water and coastal aquifers after Na-Cl since they occur in close association with carbonates, hence it is probably the reason why Mg and SO_4 show very good correlation in this study. When looking at Figure 21-e, the spring water samples show a higher affinity towards sulphate enrichment by plotting very close to and above the 1:1 equiline particularly TC-01, TC-02, UM-S and BH-01 – all which are CO_2-rich, whereas the CO_2-poor BH-02 indicates a discrepancy by being depleted in SO_4.

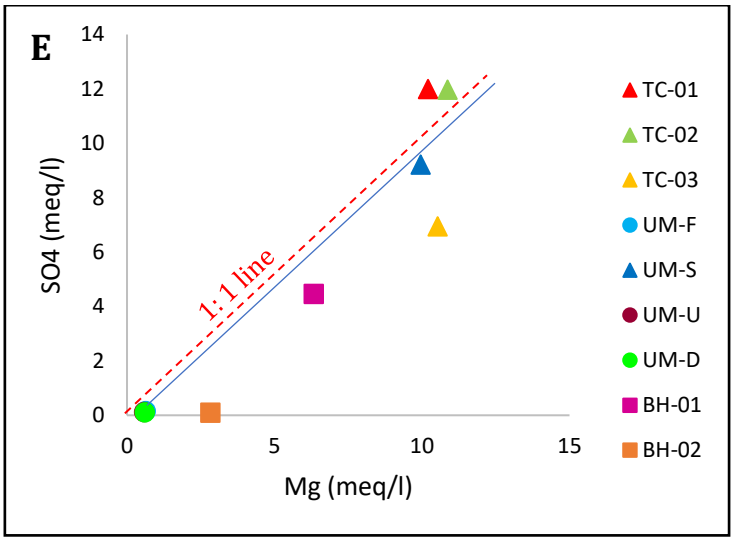

Figure 21-e: Mg vs SO_4 bivariate plot for the analysed water samples.

6.3. Geochemical modelling

6.3.1. Mineral Saturation Indices

Tables 13 and 14 show mineral Saturation Indices (SIs) that were calculated using PHREEQC Interactive modelling programme (Parkhurst and Appelo, 1999) and Visual MINTEQ v3 (Gustafsson, 2000) based on the groundwater chemistry data in Table 9 as input data. The purpose of using two different modelling software was to improve the quality (accuracy) of the results and to check for mineral phases that might have been misrepresented. The SIs were calculated to display the saturation state of mineral phases and to complement the information discussed regarding the source of chemical constituents detected in the groundwater of the study area.

When looking at the SI results in Tables 13 and 14, since SiO_2 was not analysed for this study, mineral phases that includes silica (Equations 13 and 14) are not represented in the SI results. The absence of silica mineral phases in the input data subsequently resulted in the overemphasis or oversaturation of aluminium mineral phases (Gibbsite). This is the aluminium that would have otherwise been incorporated into the structure of the kaolinite phase.

Table 13: Saturation indices determined using Visual MINTEQ

Phases	Formula	TC-01	TC-02	TC-03	UM-S	BH-01	BH-02
Anhydrite	$CaSO_4$	-1.32	-1.01	-1.20	-1.11	-1.88	-3.68
Aragonite	$CaCO_3$	0.39	0.62	0.76	0.56	-0.87	-0.88
Artinite	$Mg_2(OH)_2CO_3 \cdot 3H_2O$	-5.52	-6.03	-5.93	-6.06	-8.36	-7.24
Brucite	$Mg(OH)_2$	-5.24	-5.64	-5.68	-5.62	-7.05	-5.95
Calcite	$CaCO_3$	0.53	0.77	0.90	0.71	-0.72	-0.74
Dolomite	$CaMg(CO_3)_2$	2.18	2.42	2.97	2.23	-2.39	-2.39
Epsomite	$MgSO_4 \cdot 7H_2O$	-3.38	-3.42	-3.61	-3.51	-3.72	-5.49
Fluorite	CaF_2	-0.009	0.26	0.06	0.35	-2.10	-2.02
Gibbsite	$Al(OH)_3$	1.61	0.61	2.04	1.49	0.79	0.59
Gypsum	$CaSO_4 \cdot 2H_2O$	-1.07	-0.76	-0.95	-0.86	-1.63	-3.43
Halite	NaCl	-4.56	-4.57	-4.94	-4.80	-5.89	-6.05
Magnesite	$MgCO_3$	-0.31	-0.43	-0.29	-0.47	-1.35	-1.33
Nesquehonite	$Mg(HCO_3)\,(OH) \cdot 2H_2O$	-3.10	-3.22	-3.09	-3.26	-4.14	-4.12

Table 14: Saturation indices determined using PHREEQC

Phases	Formula	TC-01	TC-02	TC-03	UM-S	BH-01	BH-02
Anhydrite	$CaSO_4$	-1.37	-1.06	-1.26	-1.16	-1.95	-3.76
Barite	$BaSO_4$	-0.43	-0.48	-0.45	-0.67	0.23	-1.45
Calcite	$CaCO_3$	0.65	0.88	1.01	0.82	-0.62	-0.64
CO_2 (g)	CO_2	-1.40	-1.11	-0.94	-1.17	-0.62	-1.71
Dolomite	$CaMg(CO_3)_2$	1.60	1.72	1.96	1.61	-0.73	-0.73
Fluorite	CaF_2	0.14	0.42	0.21	0.51	-1.96	-1.91
Gibbsite	$Al(OH)_3$	0.96	-0.29	1.43	0.90	0.00	-0.06
Gypsum	$CaSO_4 \cdot 2H_2O$	-1.07	-0.75	-0.95	-0.86	-1.65	-3.46
Halite	NaCl	-4.57	-4.58	-4.95	-4.81	-5.90	-6.07
Rhodochrosite	$MnCO_3$	-1.27	0.26	0.50	0.32	-0.07	-0.39
Witherite	$BaCO_3$	-3.89	-4.03	-3.67	-4.17	-3.93	-3.82

There are differences in the mineral phases represented by both software programmes. Visual MINTEQ is more geared strictly towards Mg-rich mineral phases and hence included unique phases such as artinite, magnesite, epsomite and Nesquehonite – all of which are not represented by PHREEQC. These magnesium salts are known to occur in association with carbonate precipitates in caves and groundwater systems (Ruiz-Agudo *et al*. 2007). However, PHREEQC has unique phases such as barite, witherite and most importantly, it represented the CO_2 phases which proves useful for analysis purposes in this study.

The SI results showed an under-saturation of barite, anhydrite, epsomite and gypsum as sulphate mineral phases. Halite as one of the typical evaporite minerals is also undersaturated in all the analysed groundwater samples. It thus dissolves to give off the Na and Cl present in the groundwater.

In regards to carbonate mineral phases, calcite and dolomite are oversaturated with respect to the solution in which they are contained in all the Umtamvuna spring samples (TC-01, TC-02, TC-03 and UM-S) and form travertine deposits on the surface due to precipitation from these supersaturated fluids as aqueous CO_2 degasses. CO_2 is undersaturated in all the samples since most of it reacts to form HCO_3 ions as temperature increases. The Bongwana borehole water samples (BH-01 and 02) indicated undersaturated carbonate mineral phases, implying carbonate dissolution to give off CO_2. This holds true since there are no travertine deposits on the surface where sampling was done except the CO_2 degassing in BH-01 while BH-02 is CO_2-poor. These results provide more evidence that proves the influence of carbonates on the chemistry of the groundwater in the study area.

Rhodochrosite is oversaturated in most of the Umtamvuna samples except in TC-01 and in all Bongwana samples. Its potential for precipitation serves as a possible reason why only small Mn was detected in the analysed groundwater samples. Magnesite, nesquehonite, magnesite, epsomite and witherite are all undersaturated with respect to the solutions in which they are contained. However, fluorite showed a general oversaturation in all the Umtamvuna samples and is undersaturated in Bongwana samples. Withers (2012) state that fluorite is a typical minor constituent in a carbonate system.

Chapter 7: Conclusions and Recommendations

This research was conducted along the Bongwana Fault, which runs across several areas, but can be best studied at Umtamvuna in Bizana, Eastern Cape and Bongwana, Kwa-Zulu Natal. These two areas are characterised by sites of natural CO_2 release and are, therefore, assumed to be situated along the Bongwana gas fault zone. The $\delta^{18}O$ and $\delta^{2}H$ results indicated a clear distinction between the spring waters, borehole water and stream water based on their openness or seclusion from the open atmosphere. Furthermore, there is mixing of connate and recent recharge waters. Based on the 14C mean residence time, the groundwater in the study area are substantially old. On the other hand, the results from d-excess, isotopes and major ion analyses revealed that the Umtamvuna River does not have any influence (there is no connection) on the spring water compositions as far as the groundwater recharge of the area is concerned. As such, there is no indication of mixing of springs groundwater and river water compositions.

The source of CO_2 was investigated using $\delta^{13}C$ which confirmed carbonate dissolution as the main source. The results further showed that the source of CO_2 detected in the groundwaters of the study area is the reaction of acidic groundwater with carbonates at depth. The evidence is compelling since there is a presence of Marble Delta Formation consisting of calcitic and dolomitic marbles currently being mined approximately 30 km NE of the study area. Therefore, it is possible that the same rocks underlie the Dwyka Group and subsequently occur below the Bongwana Fault. The analysed results indicated that carbonate dissolution results in the formation and degassing of CO_2, and carbonate reprecipitation – a process that is interchangeable depending on the favourable conditions, i.e. pH, saturation of the solution, temperature and most importantly – pCO_2. Increased pCO_2 makes the carbonate rock more soluble and susceptible to dissolution when it encounters acidic groundwater at depth, forming CO_2 which later degasses upon being in contact with the lower atmospheric CO_2 pressure. As the pCO_2 decreases, the supersaturated (CO_2-rich) water will allow travertine to begin precipitating out of solution. The Saturation Indices indicated that that calcite is oversaturated in the Umtamvuna spring water samples, as an indication of travertine formation, whereas calcite is undersaturated in the Bongwana borehole water samples, as an indication of CO_2 exhalation for BH-01 since there are no travertine detected.

When looking at the HCO_3 and pH of the CO_2-rich groundwater in the study area, the pH is normally buffered during the process of carbonate dissolution, which neutralises the acidic groundwater. Hence, the field pH values gradually rise to be more than 7.00 despite the consistent presence of CO_2 which reacts reversibly to form carbonic acid when dissolved in water (see the lab pH values in Table 9).

The depositional environment for the main aquifer in the study area (Msikaba Formation sandstone) is an ancient marine environment where connate waters were trapped during sediment deposition and are now preserved in selected locations where later fresh groundwater influx is poor. Hence, provided the source of high salinity (mainly from halite where Saturation Indices shown to be dissolving) and sulphate detected, accompanied by EC values >400 mS/m for CO_2-rich waters. Furthermore, the estimated ratios indicated that cation exchange is prevalent and thus, it is highly possible that gypsum and epsomite are also contributing to the salinity as well as excess Ca and Mg detected in the analysed waters. Hence, the dominant water facies types are Na-Ca-Cl-HCO_3 and Na-Mg-HCO_3-Cl-SO_4 respectively.

Silicate weathering could not be modelled using PHREEQC and Visual Minteq modelling software for Saturation Indices since SiO_2 was not analysed for this study. However, evidence of plagioclase feldspar silicate weathering was provided by kaolinization of tillite rocks marking the faulting in some parts along the Bongwana Fault by CO_2-rich fluids. Water-rock interaction ratio calculations also provided evidence which supports this process.

Recommendations

SANEDI and CGS as the principal custodians of the study area should ensure that:

- Sampling in the study area should be done seasonally in order to assess the impact of seasonal variations on water chemistry.
- Ground magnetics (or aeromagnetic survey with a reduced line-spacing for increasing the data resolution) and gravity surveys should be done, and data be made accessible for accurately mapping local fractures and faults.
- U-Pb dating or any other dating technique with longer half-life should be employed to determine the ages of the waters in the study area since the Marble Delta Formation rocks are older than ~50 000 years.
- Drilling should be conducted to acquire drill core samples that can be used to support geophysical data and geological analyses.
- More boreholes should be drilled around the two localities in order to acquire more groundwater samples that can be used to improve the quality of results obtained.

References

Abiye, T. A. (2013). The use of isotope hydrology to characterize and assess water resources in South (ern) Africa. Water Research Council (WRC), Technical report TT 570/13, 1 – 211 pp.

Abiye, T. A., Bybee, G. and Leshomo, J. (2018). Fluoride concentrations in the arid Namaqualand and the Waterberg groundwater, South Africa: Understanding the controls of mobilization through hydrogeochemical and environmental isotopic approaches, *Groundwater for Sustainable Development*, **vol. 6**, 112 – 120 pp.

Appelo, C. A. J. and Postma, D. (1996). Geochemistry, groundwater and pollution. Rotterdam: Balkema

Appelo, C. A. J. and Postma, D. (2005). Geochemistry, groundwater and pollution. (2nd edition). Rotterdam: Balkema.

Beck, B., Surridge, T. and Hietkamp, S. (2013). The South African Centre for Carbon Capture and Storage Delivering CCS in the Developing World, *Energy Procedia*, **37**, 6502 – 6507 pp.

Bond, C.E., Wightman, R. and Ringrose, P.S. (2013). The influence of fracture anisotropy on CO_2 flow. *Geophys. Res. Lett*. **40 (7)**, 1284–1289 pp.

Bond, C. E., Johnson, G., Hicks, N., Kremer, Y., Gilfillan, S. M. V., Jones, D. G., Lister, R., Maupa, T., Munyangane, P., Robey, K., Saunders, I., Shipton, Z. K., Pearce, J. and Haszeldine, R. S. (2016). Fracture-controlled CO_2 gas migration at the Bongwana natural CO_2 release site, *Conference Paper*, 1-2 pp.

Bond, C. E., Kremer, Y., Johnson, G., Hicks, N., Lister, R., Jones, D. G., Haszeldine, R. S., Saunders, I., Gilfillan, S. M. V., Shipton, Z. K. and Pearce, J. (2017). The physical characteristics of a carbon dioxide seeping fault: The implications of fracture permeability for carbon capture and storage integrity, *International Journal of Greenhouse Gas Control*, **vol. 60**, 49–60 pp.

Busakwe, N. S. (2015). Stratigraphy and sedimentology of the Msikaba Formation in Kwa-Zulu Natal south coast, South Africa. University of Fort Hare, Master of Science Dissertation, *DSpace Repository*, 175 pp.

Chacko, T., Mayeda, T. K., Clayton, R. N. and Goldsmith, J. R. (1991). Oxygen and carbon isotope fractionation between CO_2 and calcite. *Geochim. Cosmochim. Acta*, **55**, 2867 – 2882 pp.

Clark, I. D. and Fritz, P. (1997). Environmental Isotopes in Hydrogeology. Lewis Publishers, New York, 1 – 352 pp.

Clark, I. D. (2015). Groundwater geochemistry and isotopes. Boca Raton, FL: CRC Press.

Climate Data (2018). Climate: Harding. [WWW] https://en.climate-data.org/location/26814/ (Accessed 19th August 2018).

Christiansen, R. L. (2001). The quaternary and Pliocene Yellowstone plateau volcanic field of Wyoming, Idaho, and Montana, *U.S. Geological Survey Professional Paper*, 729-G.

Craig, H. (1961). Isotopic variation in meteoric waters. *Science*, **133**, 1702 – 1703 pp.

Dansgaard, W. (1964). Stable Isotopes in Precipitation. *Tellis*, **16**, 436 – 468 pp.

De Decker, R.H., (1981). Geology of the Kokstad Area. **Explan Sheet 3028**. Dep. Miner. Energy Affairs, Pretoria.

Dingman, L. (2008). Physical Hydrogeology (2nd Edition), Waveland Pr Inc., New York, 1 – 1600 pp.

Dingle, R.V. and Scrutton, R.A. (1974). Continental break-up and the development of post-Palaeozoic sedimentary basins around southern Africa. *Bull. Geol. Soc. Am.* **85**, 1467–1474 pp.

Doel, S. L. (1995). Cango Caves stable isotope stratigraphy. BSc (Hons) thesis (unpubl.), University of Cape Town, 1 – 45 pp.

Duncan, R. A., Hooper, P. R., Rehacek, J., Marsh, J., and Duncan, A. R., (1997). The Timing and Duration of the Karoo Igneous Event, Southern Gondwana. *Journal of Geophysical Research*, **vol. 102 (B8)**, 18,127 – 18,138 pp.

du Toit, A.L., (1920). The Geology of Pondoland and portions of Alfred and Lower uMzimkhulu Counties, *Natal. Expl.* Sheet 28 (Pondoland), Union Geol. Survey Publ.

du Toit, A.L., (1946). The Geology of Parts of Pondoland, East Griqualand. Explanation, Cape Sheet 35. Geological Survey of South Africa.

Ehleringer, J. R., Hall, A. E. and Farquhar, G. D. (1993). Stable Isotopes and Plant Carbon-water Relations. Elsevier Inc, New York, 1 – 555 pp.

Ferguson, G and Gleeson, T. (2012). Vulnerability of coastal aquifers to groundwater use and climate change, *Nature Climate Change*, **2**, 342 – 345 pp.

Fischer, D. (2011). Why carbon dioxide (CO_2) is a Greenhouse gas [Online] https://www.scientificamerican.com/article/why-carbon-dioxide-is-greenhouse-gas/ (Accessed on the 5th November 2017).

Fitts, C. R. (2002). Groundwater Science. Academic Press Publishers, Amsterdam, 1 – 449 pp.

Garrels, R. M. and Mackenzie, F. T. (1971). Evolution of sedimentary rocks: A new approach to the study of material transfer and change through time. New York: W.W. Norton & Co.

Gavenas, E., Rosendahl, K, Skjerpen, T. (2015). CO_2-emissions from Norwegian oil and gas extraction, *Energy*, **90**, 1956 – 1966 pp.

Gevers, T.W., (1941). Carbon dioxide springs and exhalations in Northern Pondoland Alfred County Natal. Trans. *Geol. Soc. S. Afr.* **44**, 233–301 pp.

Geyh, M. A. (2000). Environmental isotopes in the hydrological cycle: Principles and applications. *International Atomic Energy Agency and United Nations Educational, Scientific and Cultural Organization*, **vol. 4**, 311 – 424 pp.

Goldich, S.S. (1938). A study in rock weathering. *Journal of Geology*, **46 (1)**, 17 – 58 pp.

Grab, S. and Knight, J. (2015). Landscapes and landforms of South Africa – an overview. In: Grab, S., Knight, J. (Eds.), Landscapes and Landforms of South Africa. *World Geomorphological Landscapes. Springer, Switzerland*, 186 pp.

Gustafsson, J. P. (2000). Visual MINTEQ version 3.1 [Online] https://vminteq.lwr.kth.se/ (Accessed 8th June 2018).

Harris, C., Stock, W. D. and Lanham, J. (1997). Stable isotope constraints on the origin of CO_2 gas exhalations at Bongwan, Natal. *South African Journal of Geology*, **100 (3)**. 261 – 266 pp.

Hartnardy, C. J. H. (1985). Uplift, faulting, seismicity, thermal spring and possible incipient volcanic activity in the Lesotho-Natal region, SE Africa. *Tectonics*, **vol. 4**, 371-377 pp.

Haase, C., Dethlefsen, F., Ebert, Ma. and Dahmke, A. (2013). Uncertainty in geochemical modelling of CO_2 and calcite dissolution in NaCl solutions due to different modelling codes and thermodynamic databases. *Applied Geochemistry*, **33**, 306 – 317 pp.

Hicks, N. (2010). Extended distribution of Natal Group within southern KwaZulu-Natal, South Africa. Implications for sediment sources and basin structure. *South African Journal of Geology*, **113**, 287-306 pp.

Hicks, N., Johnson, G., Bond, C. E., Gilfillan, S. M. V., Jones, D. G., Kremer, Y., Lister, R., Maupa, T., Munyangane, P., Robey K., Saunders, I. and Nkwane, M. (2014). The Bongwana natural CO_2 release, *Council for Geosciences presentation*, 14 pp.

Hicks, N. (2015). Preliminary CO_2 emissions monitoring on natural CO_2 releases in KwaZulu-Natal. *Council for Geosciences Geoclips*. **Vol. 43**, 1–8 pp.

Hirt, C., Filmer, M. S. and Featherstone, W. E. (2010). Comparison and validation of recent freely-available ASTER-GDEM ver1, SRTM ver4.1 and GEODATA DEM-9S ver3 digital elevation models over Australia. *Australian Journal of Earth Sciences*. **57 (3),** 337–347 pp.

Hiscock, K. M. (2005). Hydrogeology: Principles and Practice. Blackwell Publishers, United Kingdom, 1 – 405 pp.

Hobba, W.A., Fisher, D. W., Pearson, F. J. and Chemerys, J. C. (1979). Hydrology and geochemistry of thermal springs of the Appalachians, *Geological Survey Professional Paper*, 1044-E, 1 – 36 pp.

Hounslow, A.W. (1995). Water quality data: Analysis and interpretation. New York: Lewis Publishers, 1 – 416 pp.

Jalali, M. (2007). Assessment of the chemical components of Famenin groundwater, *Western Iran. Environmental Geochemistry and Health*, **29 (5)**, 357 – 374 pp.

Johnson, G., Hicks, N., Bond, C. E., Gilfillan., S. M. V., Jones, D. G., Kremer, Y., Lister, R., Nkwane, M., Maupa, T., Munyangane, P., Robey, K., Saunders, I., Pearce, J., Shipton, Z. K. and Haszeldine, R. S. (2017).

Detection and understanding of natural CO_2 releases in KwaZulu-Natal, South Africa, *Greenhouse control and Technology*, **13**, 1-7 pp.

Johnson, M.R., Anhaeusser, C.R. and Thomas, R.J. (2006). The Geology of South Africa. Geological Society of South Africa, Johannesburg/Council for Geoscience, Pretoria, 691 pp.

Kretzmann, S. (2017). SA coal to dominate as African demand expands. [Online] https://www.fin24.com/Economy/sa-coal-to-dominate-as-african-demand-expands-20170203 (Accessed 23rd January 2019).

Kura, N. U., Ramli, M. F., Sulaiman, W. N. A., Ibrahim, S., Aris, Z. and Mustapha, A. (2013). Evaluation of factors influencing the groundwater chemistry in a small tropical island of Malaysia. *International Journal of Environmental Research and Public Health*, **10 (5)**, 1861 – 1881 pp.

Ledesma-Ruiz, R., Pasten-Zapata, E., Parra, R., Harter, T. and Mahlknecht, J. (2015). Investigation of the geochemical evolution of groundwater under agricultural land: A case study in north-eastern Mexico, *Journal of Hydrology*, **521**, 410 – 423 pp.

Liu, Y., Zhou, X., Fang, B., Zhou, H. and Yamanaka, T. (2012). A preliminary analysis of the formation of travertine and travertine cones in the Jifei hot spring, Yunnan, China, *Environ. Earth Sci.*, **66**, 1887 – 1896 pp.

Liu, Z., Dreybrodt, W. and Liu H. (2011). Atmospheric CO_2 sink: Silicate weathering or carbonate weathering? *Applied Geochemistry*, **26**, 292 – 294 pp.

Merkel, B. J. and Planer-Friedrich (2008). Groundwater chemistry: A practical guide to modelling natural and contaminated aquatic systems (2nd Edition). *Springer*, Germany, 1 – 230 pp.

Metz, B., Davidson, O., de Connick, H. C., Loos, M. and Meyer, L. A. (2005). IPCC Special Report on Carbon Dioxide Capture and Storage. Prepared by Working Group III of the Intergovernmental Panel on Climate Change. Cambridge, United Kingdom and New York, NY, USA, *Cambridge University Press*. 1 – 35 pp.

Moore, J. G., Bachlader, N. and Cunningham, C. G. (1977). CO_2-filled vesicles in mid-ocean basalt. *J. volcanol. geothermal res*. **2**, 309 – 327 pp.

Nkwane, M. 2018. Hydrogeochemical and environmental isotope characterization of the CO_2 springs along the Bongwana Fault: Its impact on freshwater resources and implications for CCS in South Africa. MSc Dissertation, UKZN, 1 – 96 pp.

Nolan, T. B. (1962). Chemistry of iron in natural waters. U.S Geological Survey, *United States Government Printing Office*, 1 – 39 pp.

Otto, J.D.T. (1973). The Geology and Petrology of the Marble Delta. PhD Thesis. University of Stellenbosch, 1 – 174 pp.

Paige-Green, P. 1980. The clay mineralogy of Dwyka tillite in Southern Africa and its effect of geotechnical properties. *South African Journal of Geology*, **83 (2)**, 291 – 296 pp.

Parkhurst, D. L. and Appelo, C. A. J. (1999). User's guide to PHREEQC (Version 2) – A computer program for speciation, batch-reaction, one-dimensional transport, and inverse geochemical calculations. U.S. Department of the Interior.

Parkhurst, D.L. and Appelo, C. A. J. (2012). Description of input and examples for PHREEQC (Version 3): A Computer program for speciation, batch-Reaction, one-dimensional transport, and inverse geochemical calculations. *Water-Resources Investigations Report* 99-4259. Denver. Colorado: U.S. Department of the interior & U.S. Geological Survey.

Plummer, L. N. (1992). Geochemical Modelling of Water-Rock Interaction: Past, Present, Future," in Water-Rock Interaction, **Vol. 1**, Kharaka, Y. K. and Maest, A. S. (Eds.), Balkema, Rotterdam, Brookfield, 1 – 858 pp.

Pentecost, A. (2005). Travertine. *Springer Publishers*, United Kingdom, 1 – 48 pp.

Rinaldi, A.P. and Rutqvist, J. (2013). Modelling of deep fracture zone opening and transient ground surface uplift at KB-502 CO_2 injection well, In Salah, Algeria. *Int. J. Greenh. Gas Control*, **12**, 155–167 pp.

Ringrose, P.S., Mathieson, A.S., Wright, I.W., Selama, F., Hansen, O., Bissell, R., Saoula, N. and Midgley, J. (2013). The In-Salah CO_2 storage project: lessons learned and knowledge transfer. *Energy Procedia*, **37**, 6226–6236 pp.

Roberts, J. J., Wood, R. A., Wilkinson, M. and Haszeldine, S. (2015). Surface controls on the characteristics of natural CO_2 seeps: implications for engineered CO_2 stores. *Geofluids*, **15**, 453 – 463 pp.

Ruiz-Agudo, E., Martin-Ramos, J. and Rodriguez, C. (2007). Mechanism and kinetics of dehydration of epsomite crystals formed in the presence of organic additives, *J. Phys. Chem*, **111**, 41 – 52 pp.

Ryan, P. C. (2014). Environmental and low temperature geochemistry. *Wiley Blackwell Publishers*, United States, 1 – 402 pp.

Salem, O., Visser, J. M., Deay, M. and Gonfiantini, R. (1980). Groundwater flow patterns in the western Libyan Arab Jamahiriya evaluated from isotope data", Arid Zone Hydrology: Investigations with Isotope Techniques, IAEA, Vienna, 165 – 179 pp.

Santo, R. V. and Clayton, R. N. (1995). Variations of oxygen and carbon isotopes in carbonatites: A study of Brazilian alkaline complexes. *Geochimica et Cosmochita Acta*, **59 (7)**, 1339 – 1352 pp.

Scheiber-Enslin, S., Ebbing, J. and Webb, S. (2014). An integrated study geophysical study of the Beattie magnetic anomaly, South Africa. *Tectonophysics*, **636**, 228 – 243 pp.

Schoeller, H. (1977). Geochemistry of groundwater. (Chapter 15). In Groundwater studies—an international guide for research and practice. Paris: *UNESCO*, 1 – 18 pp.

Steiger, M., Linnow, K., Ehrhardt, D., and Rohde, M. (2011). Decomposition reactions of magnesium sulfate hydrates and phase equilibria in the MgSO4-H2O and Na+-Mg2+-Cl--SO42--H2O systems with implications for Mars. *Geochimica et Cosmochimica Act*, **75 (12)**, 3600 – 3626 pp.

Thomas, R. J., (1988). The Geology of the Port Shepstone Area. Explanation of Sheet3030 (1:250000). Geological Survey of South Africa, 136 pp.

Thomas, R. J., von Brunn, V., Marshall, C.G.A. (1990). A tectono-sedimentary model for the Dwyka Group in southern Natal, South Africa. *South African Journal of Geology*, **93**, 809–817 pp.

Thomas, R. J. and Otto, J. D. T. (1991). Marble Delta Formation [uMzimkhulu Group], Catalogue of South African Stratigraphic Units (SA Committee for Stratigraphy).

Thornhill, M. and van Vuuren, D. (2015) Strategic Environmental Assessment for the Umuziwabantu Local Municipality, KwaZulu-Natal: SEA Analysis Report. Draft in Prep, Thorn-Ex Ref C055, Pietermaritzburg.

Urban Earth (2012). ESKOM announces unchanged electricity emission factor for 2012 [Online] http://www.urbanearth.co.za/articles/eskom-announces-unchanged-electricity-emission-factor-2012 (Accessed on the 5th November 2017).

Walraevens, K., Cardenal, J. and Van Camp, M. (2007). Reaction transport modelling of a freshening aquifer (Tertiary Ledo-Paniselian Aquifer, Flanders-Belgium). *Applied Geochemistry*, **22**, 289 – 305 pp.

Watkeys, M.K. and Sokoutis, D. (1998). Transtension in southeast Africa during Gondwana break-up. In: Holdsworth, R.E., Strachan, R., Dewey, J.F. (Eds.), Continental Transpressional and Transtensional Tectonics, *Special Publication of the Geological Society of London*, **103**, 203–214 pp.

Watkeys, M.K. (2006). The break-up of Gondwana: A South African perspective. In: Johnson, M.R, Anhaeusser, C.R. and Thomas, R. (eds.): The Geology of South Africa. Geological Society of South Africa and Council for Geoscience, 531-539 pp.

Weaver, J.M.C., Cavé, L.C. and Talma, A.S. (2007). Groundwater Sampling: A Comprehensive Guide for Sampling Methods, 2nd ed. *Water Research Council*, WRC Report No. TT 303/07, Pretoria, 1 – 183 pp.

Withers, N. (2012). Fluorine found in nature [WWW] https://www.chemistryworld.com/research/fluorine-finally-found-in-nature/5206.article (Accessed 15th October 2018).

Young, R. B. (1924). Exhalations of Carbon Dioxide in Alfred County, Natal. *Transactions of the Geological Society of South Africa*, **26**, 99 – 102 pp.

Zak, K., Richter, D. K., Filippi, M., Zivor, R., Deininger, M., Mangini, A. and Scholz, D. (2012). Coarsely crystalline cryogenic cave carbonate – a new archive to estimate the Last Glacial minimum permafrost depth in Central Europe, *Clim. Past*, **8**, 1821–1837 pp.

Zhu, C. and Anderson, G. (2002). Environmental Applications of Geochemical Modelling. *Cambridge University Press*, New York, USA, 1 – 300 pp.

Zhu, C. (2009). Geochemical modelling of reaction paths and geochemical reaction networks. *Reviews in Mineralogy and Geochemistry*, **70 (1)**: 533 – 569 p